U.PORTO
FEUP FACULDADE DE ENGENHARIA
UNIVERSIDADE DO PORTO

Fraunhofer
IWS

SEPTEMBER 2018

THE INFLUENCE OF PROCESSING PARAMETERS ON INCONEL 718 PARTS:

CORRELATION OF CT MEASUREMENTS WITH PROPERTIES

ANA PATRÍCIA PEREIRA MARQUES

MASTERS DISSERTATION PRESENT TO
FACULDADE DE ENGENHARIA DA UNIVERSIDADE DO PORTO IN
ENGENHARIA METALÚRGICA E DE MATERIAIS

SUPERVISOR
ELSA WELLENKAMP DE SEQUEIROS

INSTITUCIONAL SUPERVISOR
ELENA LOPEZ

CANDIDATO		Código	
TÍTULO			
DATA	__ de _____ de _____		
LOCAL	Faculdade de Engenharia da Universidade do Porto - Sala _____ · __:__h		
JÚRI	Presidente		DEMM/FEUP
	Arguente		DEM/FEUP
	Orientador		DEMM/FEUP

Abstract

Additive manufacturing technology is being dramatically developed and brings new potential applications into industry. For high-quality products that are used in demanding industries it's essential to verify that all the requirements are fulfilled, and this is possible using quality control (QC) methods. Computer Tomography (CT) is a promising technique for AM's QC, and in this way, in this research its capacities and measure accuracy were evaluated. Besides, to exploit the whole potential of AM, it's essential to investigate the complex relationships between AM process, the resulting microstructure and mechanical properties. In this way, the laser powder bed fusion process (LPBF) is investigated in order to understand how its parameters, namely, laser power (LP), distance hatch (DH), point distance (PD) and exposure time (ET), influence the microstructure and mechanical properties in Inconel 718 parts, built in the horizontal and vertical direction. For this, several tests were used to evaluated the specimens produced namely, Computer Tomography (CT), Optical Microscopy (OM), Scanning Electron Microscope (SEM)/Electron Backscatter Diffraction (EBSD) and tensile tests. Regarding the results, CT technique has shown to be a good benefit in the AM field because through the comparison with other common methods its results were mostly in accordance, having the advantage of being a non-destructive method. The tensile tests results showed that the horizontal direction presents higher ultimate tensile strength (UTS) and lower elongation percentages and the vertical direction has the inverse properties. The relationship between building orientation and mechanical properties is mainly attributed to the different amount of residual stress due to thermal gradients and internal defects. Moreover, the amount of internal defects, such us, porosity, affects mainly the ductility percentage and not the UTS value. In this way, the higher the porosity value the lower the ductility. The microstructure showed a very fine cellular-dendritic structure, the different melt pool boundaries and, lastly, the grain growth direction in each building orientation.

Keywords

Resumo

A tecnologia de fabricação aditiva (FA) tem apresentado um desenvolvimento significativo, trazendo novas aplicações para a indústria. De modo a que os produtos possam ser usados em indústrias exigentes, é essencial verificar se todos os requisitos são satisfeitos, e isso é possível recorrendo a métodos de controlo da qualidade (CQ). A tomografia computadorizada (TC) é uma técnica promissora para o CQ em FA e, desta forma, nesta pesquisa, as suas capacidades e incerteza da medição foram avaliadas. Além disso, para explorar todo o potencial da FA, é essencial investigar as relações complexas entre o processo FA, a microestrutura resultante e as propriedades mecânicas. Desta forma, o processo de *Laser Powder Bed Fusion* (LPBF) é investigado para entender como seus parâmetros, nomeadamente, potência do laser, distância entre camadas, distância entre pontos e tempo de exposição, influenciam a microestrutura e propriedades mecânicas em peças Inconel 718, construídas na direção horizontal e vertical. Posto isto, vários testes foram utilizados para avaliar as amostras produzidas: Tomografia Computadorizada (TC), Microscopia Óptica (MO), Microscopia Eletrónica de Varrimento (MEV) / técnica de difração de eletrões retro-difundidos (EBSD) e ensaios de tração. Relativamente aos resultados, a técnica de TC mostrou-se um bom benefício na área de FA, pois através da comparação com outros métodos, os seus resultados estavam em grande parte de acordo, tendo a vantagem de ser um método não destrutivo. Os resultados dos ensaios de tração mostraram que a direção horizontal apresenta valores de resistênica mecânica superiores e alongamento inferior e a direção vertical apresenta as propriedades inversas. A relação entre a orientação de contrução e as propriedades mecânicas é atribuída principalmente a diferenças de tensão residual resultante de gradientes térmicos e defeitos internos. Além disso, a quantidade de defeitos internos (p.e. porosidade), afeta principalmente a percentagem de ductilidade e não o valor de resistência mecânica. Desta forma, quanto maior o valor de porosidade menor a ductilidade da peça. A microestrutura apresentou uma estrutura dendrítica celular muito fina, os limites da zona de fusão e, por fim, a direção de crescimento dos grãos em cada orientação do construção.

Acknowledgements

I would like to thank first to my thesis advisor, Elsa Wellenkamp de Sequeiros, who believed in my abilities and entrusted me with this project. She consistently allowed this paper to be my own work, but steered me in the right the direction whenever she thought I needed it.

I would also like to thank to Fraunhofer Institute IWS experts, specially, to my institutional supervisor Elena Lopez for this opportunity, guidance and support and Oliver Fitzek for working alongside with me and being an incredible help during the practical work. Axel Marquardt for the formation on the computer tomography and Christoph Wilsnack for providing the samples, support with MiniTab Software and answer doubts risen during the project.

I would like to thank Joao Tomás Afonso, you've been there since the beginning and this experience was also possible because of you. Thank you for sharing your knowledge with me, hear and understand my insecurities about this project.

Finally, I must express my very profound gratitude to my parents and brother for providing me with unfailing support and continuous encouragement throughout my years of study and through the process of researching and writing this thesis.

A special thanks to my sister-in-law, Fátima Marques, besides being family, she's my best friend. All the obstacles in this journey were overcome with her unconditional support and hours on the phone. There are no words to express my gratitude.

This accomplishment would not have been possible without my friends that love, care and cherish me. Thank you.

Contents

Figure index

Table index

List of Abbreviations

AM	Additive Manufacturing
ASTM	American Society for Testing and Materials
BD	Binder Jetting
CMM	Coordinate Measuring Machine
CMSs	Coordinate Measuring Systems
CT	X-ray Computed Tomography
DED	Direct Energy Deposition
DMLM	Direct Metal Laser Melting
DMLS	Direct Metal Laser Sintering
EBM	Electron Beam Melting
EBSD	Electron Backscatter Diffraction
ED	Energy Density
ET	Exposure Time
FDD	Focus Detector Distance
FOD	Focus Object Distance
HD	Hatching Distance
HIP	Hot isostatic pressure
HoD	Horizontal Direction
ISO	International Organization for Standardization
LP	Laser Power
LPBF	Laser Powder Bed Fusion
NDT	Non-Destructive Techniques

OM	Optical Microscopy
PBF	Powder Bed Fusion
PD	Point Distance
QA	Quality assurance
QC	Quality control
SS	Scanning Speed
SEM	Scanning Electron Microscope
SLM	Selective Laser Melting
SLS	Selective Laser Sintering
Srμt	Synchrotron radiation micro-tomography
VD	Vertical direction

1. Introduction

Additive Manufacturing (AM) is a manufacturing process, which allows to build three-dimensional objects by adding materials element by element or layer by layer. This offers unique and novel approaches to product development and manufacturing. AM also enables the manufacturing of parts with complex geometries that are impossible to manufacture by conventional manufacturing processes [1, 2].

AM technology in industries has reached up to 50 per cent as prototype or end-product. However, for AM products to be directly used as final products, they should be produced through advanced Quality Control (QC) methods, which are able to prove and reach their desire repeatability, reproducibility, reliability and preciseness. Therefore, this research will focus in one of the most promising methods to control quality in AM, namely, X-ray Computed Tomography (CT). The measurements of porosity obtained by this technique will be compared to other two methods, particularly, OM (Optical Microscopic) and the Archimedes method. This is a calibration attempt and a way of evaluating the measurement uncertainty. Besides, this technique will also be indispensable to understand how the porosity varies according to the process parameters and mechanical properties [3].

Besides, in order to take advantage of AM technologies, engineers and scientists must have a good understanding of the process and the motivation for this research has also risen from the need to deepen knowledge concerning the Laser Powder Bed Fusion (LPBF) process, focusing on, proper adjustment of parameters. This is relevant because they directly influence material microstructures and its defects, affecting the final mechanical properties required for the intended applications [4]. Moreover, it's also possible to point out, based on currently researches that, the inner-defects and building orientations evidently influence the mechanical properties of AM metals, especially tensile and fatigue strength. With this it's pertinent to continue studying this variation and extend knowledge in this field [5].

In this way, this research project also aims to understand how process parameters, affect the mechanical properties and microstructure on Inconel 718 parts. The microstructure and porosity were studied using two main techniques, namely, CT and OM, identifying and quantifying the porosity percentage on the samples. When it comes to the mechanical properties, tensile tests were executed. To complement the information provided by the tensile tests and in order to understand the differences between the building orientation OM and SEM / EBSD analysis were made.

2. State of art

Throughout this research three main concepts will be addressed: LPBF (AM process) in Inconel 718 parts, their microstructure and mechanical properties, figure 1.
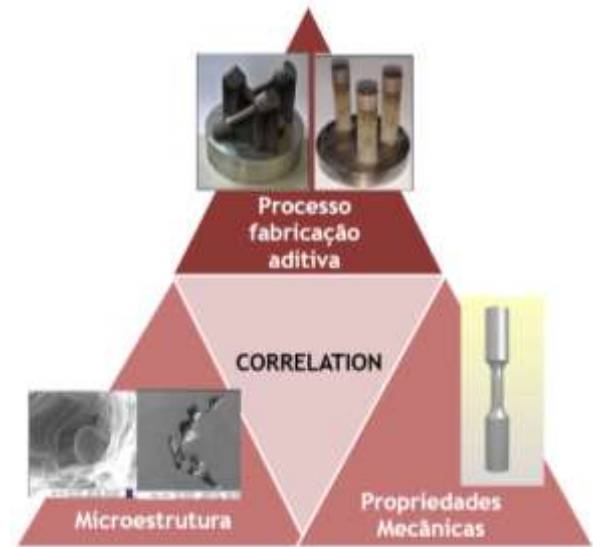
In the state of the art, firstly will be made an approach to the process and material under study. After that, it's time to think about the next step in the production cycle, quality control. That is, to check the quality of the part, proving the reliability of the product and to verify that all the requirements are fulfilled. In this way, in the last section is addressed the importance of quality control and is present a prominent technique to control the quality of parts produced by AM, CT.

2.1. Additive Manufacturing (AM)

In the recent years, metal AM processes have been gaining an increasing industrial attention for the production of functional components, ranging from one-of-a-kind to mass productions. AM is defined as the "process of joining materials to make parts from 3D model data, usually layer upon layer, as opposed to subtractive manufacturing and formative manufacturing methodologies" in the International Organization for Standardization (ISO)/American Society for Testing and Materials (ASTM) 52900:2015 standard [6] . Based on the mentioned standard, AM processes can be classified into seven categories: (1) Binder Jetting (BD); (2) Directed Energy Deposition (DED); (3) Material Extrusion; (4) Material Jetting; (5) Powder Bed Fusion (PBF); (6) Sheet Lamination; and (7) Vat Photopolymerization [4, 7].

AM's unique features allows production of complex or customized parts directly from the design without the need for expensive tooling or forms such as punches, dies or casting moulds and reduces the need for many conventional processing steps. Complex parts, true to their design can be made in one-step without the limitations of conventional processing methods (e.g. straight cuts, round holes) or commercial shapes (e.g., sheet, tubing). For these reasons, AM is now widely accepted as a new paradigm for the design and production of high performance components for aerospace, medical, energy and automotive applications [4, 7].

However, despite AM techniques have progressed greatly in recent years, the widespread adoption of AM is challenged by part quality issues, such as relatively poor part accuracy caused by the stair-stepping effect and residual stresses, undefined material properties, insufficient repeatability and consistency in the produced parts, and lack of qualification and certification. Part quality issues may also be attributed to the AM process parameter settings, so it's important to establish correlations between the AM process parameters and part characteristics, to ensure desirable part quality. All these aspects have to be taken into account, because the products available on the market must be reliable and meet all the pre-established requirements [7, 8].

All the efforts to standardize AM processes are important in order to AM being truly considered part of 4.0 industry, this means the products should be fabricated promptly, efficiently and inexpensively while meeting all stringent functional requirements. To achieve this, research is needed do deepen the knowledge related to the process and materials field [4, 9].

2.2 Laser Powder Bed Fusion (LPBF)

Most current metal additive manufacturing systems consist on the Powder Bed Fusion (PBF) type and according to ISO/ASTM52900-15, this process can be defined as an "additive manufacturing process in which thermal energy selectively fuses regions of a powder bed". Current metal PBF AM systems tend to use melting as opposed to sintering to build full-density parts. The PBF encompasses the EBM (Electron Beam Melting) and LPBF and where the main differences between them is the power source

and atmosphere used. In EBM the power source is a high-energy electron beam powered by high voltage, typically 30 to 60 kV, under vacuum atmosphere (<10^{-1} Pa). On other hand, in LPBF the power source is a laser and for atmosphere uses inert gas like argon or nitrogen to avoid metal oxidation during processing. The LPBF is also known as selective laser sintering (SLS), selective laser melting (SLM), direct metal laser sintering (DMLS) and direct metal laser melting (DMLM) [10-13].

LPBF is one of the most promising AM technologies and meets the manufacturing demands of time and cost reduction. The applications more common are: biomedical applications, tooling industry, and the aerospace sector. Many of the products currently manufactured by this technology are made in commercial machines that use a limited range of materials. Therefore, the development of more flexible machines can help to increase the range of applications of these technologies [14, 15].

Talking about its working mechanism, initially the energy from the laser is absorbed through radiation by the powder and the heat transfer produces a phase transformation. The powder changes from a solid to a liquid, forming a melt pool. Once the laser moves, this melt pool solidifies to produce a consolidated layer. When the scan finishes the geometry for the layer, the build bed is lowered and a fresh layer of powder is deposited. The process will then be repeated until the end of the build program and the part is finished. The last step, in the LPBF machine, consists in removing the loose powder in order to reveal the final part [7, 10, 16].

Metal LPBF systems have designs similar to that illustrated in Figure 2. They are composed of powder delivery and energy delivery systems. The powder delivery system comprises a piston to supply powder, a coater to create the powder layer, and a piston that holds the fabricated part. The energy delivery system is made up of a laser and a scanner system with optics that enable the delivery of a focused spot to all points of the build platform. A flow of gas (usually nitrogen or argon) passes over the powder bed with the intention to protect the part from oxygen and to clear any "spatter" and metal fumes that are created during the laser path [7, 8, 10].
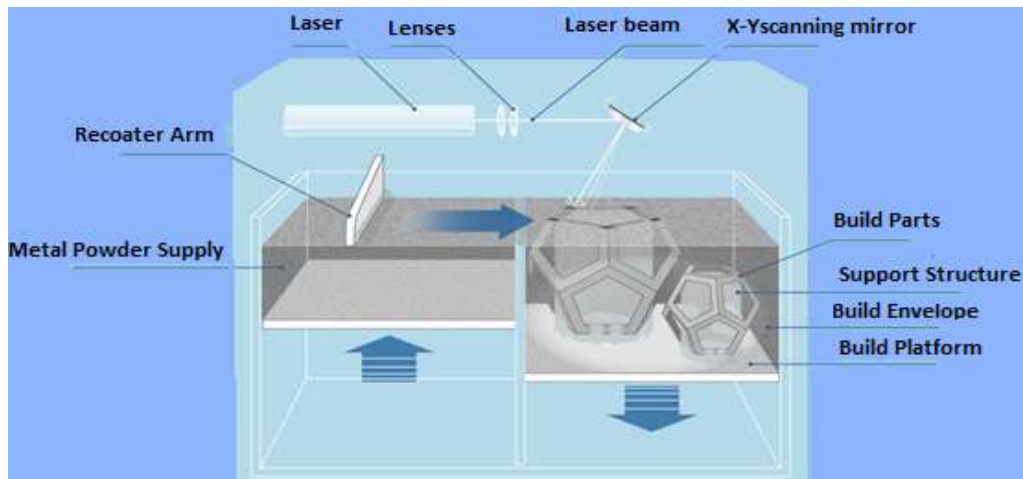
Fig. 1 - Schematics of a generic AM powder bed system [10].

As any other process, different defects can be originate in the final part, although, in some cases, post-processing techniques are suitable to mitigate or remove defects from LPBF-produced parts - e.g. HIP (Hot Isostatic Pressing) [7,14,27]. Understanding the origin of the defects and their main causes is the first step to design process monitoring and control tools. That's why, in the next section, a deeper discussion LPBF parameters, namely, laser power, distance hatch, point distance and exposure time will be detailed and explained how they affect the part's quality [8].

2.2.1 Process parameters and its influence

Every additive manufacturing process has its own process parameters that in combination with material characteristics and properties influence quality of manufacturing parts. It's currently assumed that the levels set for parameters and variations experienced during a process will contribute to dimensional inaccuracies, feature errors, porosity, layer delamination, curling and poor material properties [8, 11, 17].

Over hundred and thirty factors that affect the LPBF final parts have been defined and twenty of them are considered as important factors. However, there are ten parameters that are repeated in all literature and that can be considered controllable (i.e. laser power (LP), scanning speed (SS), layer thickness (LT), scanning space (SS)) [14, 18]. The important factors/parameters can be lumped into four categories: laser, scan, powder and temperature, which are summarize in table 1 with the correlated parameters.

Table 1 - LPBF catagorized parameters [14].

Category	Parameters
Laser - related parameters	laser power, hatch point, exposure time, pulse frequency, etc.
Scan - related parameters	scan speed, hatch spacing, and scan pattern
Powder - related parameters	particle shape, size, and distribution, powder bed density, layer thick- ness, material properties, etc.
Temperature - related parameters	powder bed temperature, powder feeder temperature, temperature uniformity, etc.

Most of these parameters are strongly interdependent and are mutually interacting. For instance, the required laser power typically increases with melting point of the material and lower powder bed temperature, and also change depending upon the absorptivity characteristics of the powder bed, which is influenced by material type and powder shape, size, and packing density [8, 17, 19].

This research will focus on the common process parameters that need to be adjusted in order to optimize the process, namely, Hatching Distance (HD), LP, Point Distance (PD), and Exposure Time (ET) Figure 3 provides an illustration of some of these process parameters [16].
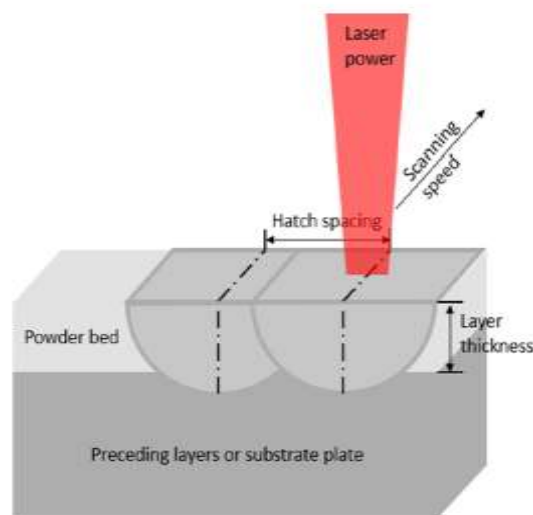
Fig. 2 - LPBF process parameters: a) laser power, scanning speed, hatch spacing, layer thickness [16].

In order to clarify the concepts under research [20, 21]:

- HD is defined as the distance between neighbor scanning vectors. It's chosen so that two adjacent lines of molten metal overlap, this overlapping is necessary to avoid the appearance of porosity;
- LP is the energy transferred to the powder in order to melt the powder particles;
- PD is the distance between the deposited spots (mm);
- ET is the time the laser is heating on one spot (s).

Together with the absorptance of powders to the laser irradiation, these parameters affect the volumetric energy density that is available to heat up and melt the powders. The laser consistency in the moment that laser meets the powder surface is also important, being one variable that is required to produce parts that are fully dense. The Energy Density (ED) is a factor that can be used to ascertain the final density of a part being produced and it relies on several factors [8, 22]:

$$Energy\ Density\ (ED) = \frac{LP}{V * HDistance * t\ layer} \tag{1}$$

Where LP = Laser power, V = scan velocity and $H_{distance}$ = hatching Distance and t_{layer} = layer thickness [8, 22].

Several studies demonstrated a correlation between the energy density and the part density and allowed the identification of a window process, where a good part density and quality is achieved. The study developed by Haijun Gong [22] outlined different regions in the parameter space spanned by laser power and scan speed in LPBF of Ti6Al4V (figure 4): zone I corresponds to fully dense parts, zone II to over-melting conditions, zone III to incomplete melting and zone OH to overheating parameters. As a result of the research concerning this subject, it was found that specimens can be built with different porosity distribution in distinct melting zones when different process parameters are used, such as laser power and scan speed. Throughout observation of figure 4 it's possible to confirm that using 120 and 80 W, the porosity distribution varies according to the laser power and, with the same laser power, in every melting zone [22].
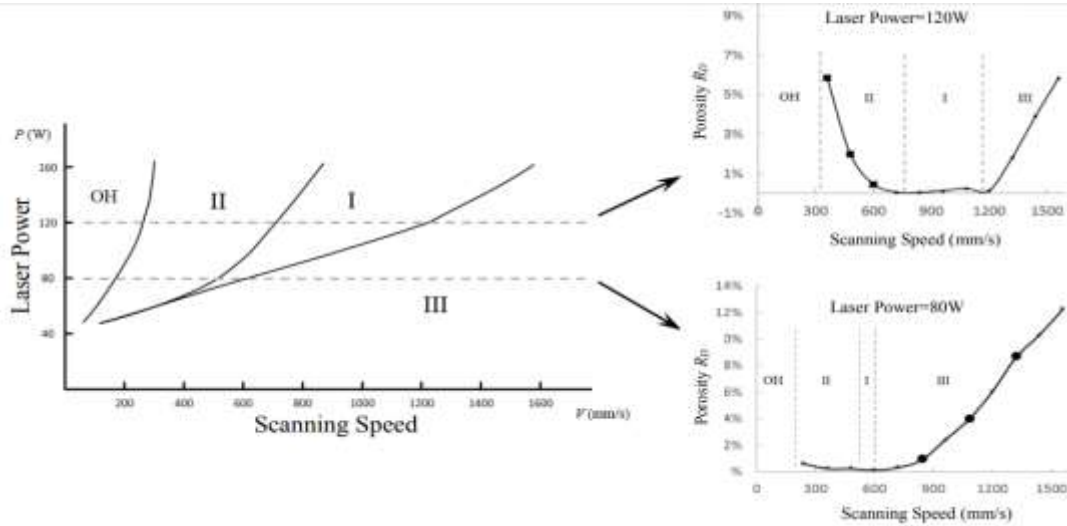
Herewith, it's reasonable to say that choosing unsuitable parameters can lead to the appearance of defects, such as, porosity. There is the need to minimize or eliminate them due to their adverse effects on mechanical properties, such as decreasing fatigue performances and influencing crack growth characteristics of the part. In this way, in the next section will be presented the main defects and discussed the relationship between the process parameters and each type of defect.

2.2.2 Defects

The defects to be addressed are, in particular, porosity, cracks and surface roughness. Thus, to facilitate these defects interpretation together with the cause of its occurrence and means for its prevention, the table 2 was constructed [23, 24].

Table 2 - Relationship between each defect (porosity, cracks and surface roughness) with cause, formation mechanism and prevention [23, 24].

	Porosity	Cracks and Delamination	Surface Roughness (balling effect)
Cause	• High laser power • High deposition rate	• high temperature gradient combined with residual stress	• Low laser power • High scanning speed • Large layer thickness
Formation Mechanism	• Keyhole mode melting • Entrapped gas • Inadequate penetration of the molten pool of an upper layer	• Thermal gradient mechanism • Cool-down phase of molten top layers	• Surface tension
Prevention	• Lower deposition rate • Lower Laser Power	• pre-heating the substrate and improve the ambient temperature	• Optimized scanning Strategy

Taking a close look to porosity formation mechanism, it's feasible to say that it can occur in three different ways. First, without careful control of keyhole mode melting, keyholes can become unstable and repeatedly form and collapse, leaving voids inside the deposit that consist of entrapped vapor (figure 5 a)). The other mechanism is related to entrapped gas inside the powder particles during the powder atomization process. In addition, gas pores may also be formed due to the entrapment of the shielding gas or alloy vapors inside the molten pool. Third, lack of fusion defects can be caused by inadequate penetration of the molten pool of an upper layer into either the substrate or the previously deposited layer [4, 24, 25]. Those voids can be found (i) within the layer part, (ii) between adjacent layers, and/or (iii) on the external surface of the part. More common pores are found within the layer, and they may have different size, shapes and spatial distributions. A distinction commonly done in the literature is between spherical pores and non-spherical pores. The voids observed between the layers are referred to as 'acicular pores' and they are characterized by an elongated shape. Figure 5 b) shows an example of two internal pores of spherical shape, and figure 5 c) one acicular pore and elongated shape [24-26]
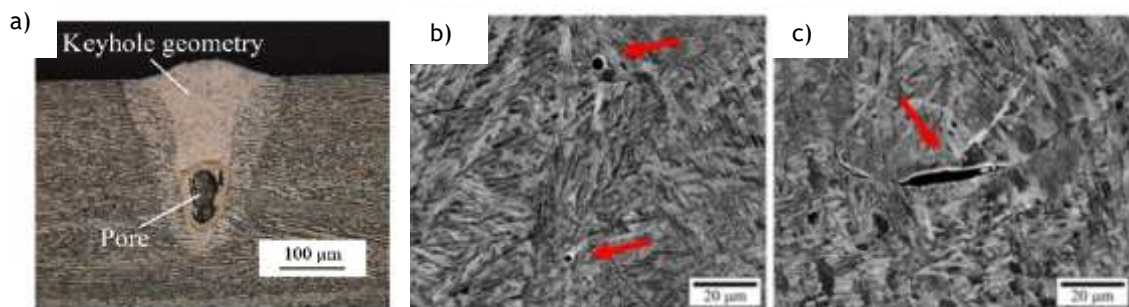
Fig. 3 - Melt pool profile (a). Example of two internal spherical pores (b) and one acicular pore (c) [24].

Another main defect in LPBF process are cracks and delamination and it occurs as a consequence of a stress relief through fracturing when the tensile stress exceeds the ultimate tensile strength of the solid material at a given point and temperature (figure 6-a)). Delamination is a particular case of cracking, where cracks originate and propagate between adjacent layers (inter-layer cracking). This kind of phenomena happens when the residual stresses exceed the binding ability between the top layer and the previous one [4, 25, 27].

The last defect to be addressed is surface roughness, being one of the outputs the melt ball formation, a.k.a. balling, and occurs when the molten material solidifies into spheres instead of solid layers, which is a severe impediment to interlayer

connection. Surface tension drives the balling phenomenon by preventing the molten material to wet the underlying layer. The result is a rough and bead-shaped surface that produces an irregular layer deposition, with detrimental effects on the density and quality of final part. The balling phenomena can bring several disadvantages: first, it can increase the surface roughness; second, a large number of pores can be formed between the discontinuous metallic balls and lastly, in case of very severe balling, the salient spheres from the powder layer may interfere with the movement of the powder deposition system. Figure 6 b) shows an example of SEM images showing the balling effect on single scan tracks corresponding to different scan speeds [24, 28].
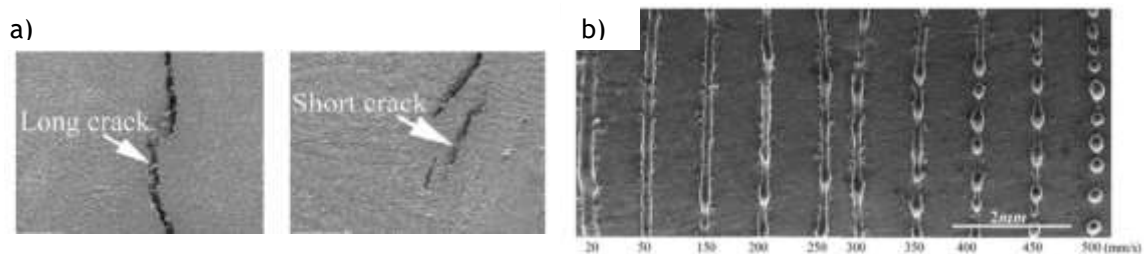
Fig. 4 - SEM images of: a) example of severe delamination and cracking. b) examples of balling effects is LPBF on single scan tracks corresponding to different scan speeds [24,28].

2.2.3 Materials

Most of the LPBF research revolves around three types of metals: steel, titanium, and nickel. These metals were selected due to their widespread application and their material cost [16, 29]. This study will focus on the analysis Inconel 718 specimens, so it's important to take a close look at their properties and applications. After steel and titanium materials, nickel-based alloy is the most studied group of metals for the LPBF process. LPBF of nickel-based superalloys, such as Inconel 718, has been studied for high temperature applications in aircraft engines as swirlers in combustion chambers, repair patches, gas turbine blades, and turbocharger rotors. Inconel 718's excellent corrosion resistance and strength at high temperatures, fatigue resistance, wear resistance, and good weldability have allowed it to be applied in several fields areas. In a review of manufacturing technologies for complex turbine blades by Lu *et al*. [30] it was highlighted that Fraunhofer ILT had used LPBF to produce turbine blades. These turbine blades had dense microstructure, high definition, and high surface quality [16, 30, 31].

Inconel 718 consists of the matrix phase γ and a variety of secondary phases. Since it is a precipitate-strengthened superalloy, the presence and distribution of secondary phases in the matrix γ are the key to determining Inconel 718's microstructure and properties. Besides, various amounts and combinations of alloying elements are also added to the γ matrix to achieve the desired microstructural features and mechanical properties (i.e Cr, Co, Al). The microstructure of additively manufactured Inconel 718 is largely dependent on the specific process history. With different process parameters, such as scanning strategy and component geometry, quite different as-manufactured Inconel 718 microstructures can be obtained even under same manufacturing method. Figure 7 presents an example of a microstructure obtained by LPBF [32].
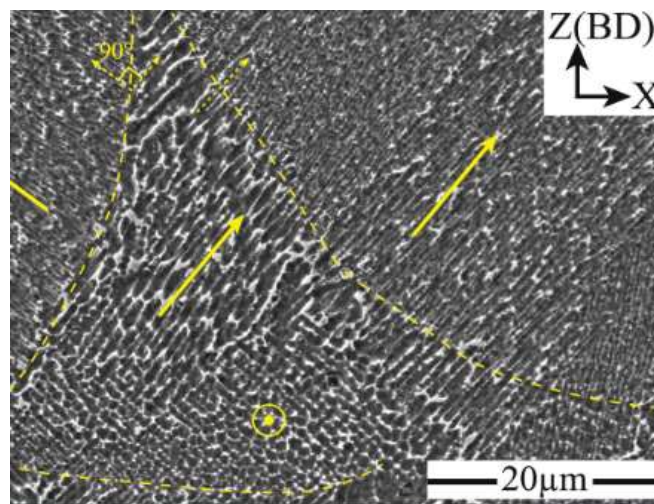
Fig. 5 - Example of the Inconel 718 microstructure manufactured by LPBF [32].

Concerning mechanical properties, in a study published by Tanja T. *et* al [33] Inconel 718 parts produced by LPBF in three different building directions (vertical, 45° and horizontal) are compared to forging and casting regarding differences in microstructure and mechanical properties. Table 3 shows the resume of these results at room temperature.

Table 3 - Reported Inconel 718 properties in LPBF, forging and casting processing [33].

	Horizontal	Vertical	45°	SLM (average)	Forged	Cast
UTS (MPa)[a]	1440	1440	1550	1430	1380	950
$R_{p0,2}$[b]	1186	1180	1190	1185	1192	940
E (%)[c]	18,5	20,4	16,9	18,6	19,1	23,1

A - Ultimate tensile strength. B - 0.2% yield strength. C – Elongation.

2.3 Quality Control

While many companies have explored the potential of AM for new business opportunities through novel designs that were previously impossible, several hurdles prevent its wider adoption, many argue that quality assurance (QA) remains the biggest issue in AM. Several manufactures and users do not have absolute confidence and certainty that AM parts would exhibit consistent quality and reliability within and across different printers and geometries [34]. Without this guarantee, manufacturers will remain leery of AM technology, judging the risks of uncertain quality to be too costly a trade-off for any gains they might realize. QA presents a multifaceted challenge, encompassing both the scale and scope of production. Indeed, quality doesn't just exist on one dimension, and each area should be addressed for parts qualification and AM's potential to be more fully realized [34, 35]. Figure 8 summarizes the major facets of AM technology.
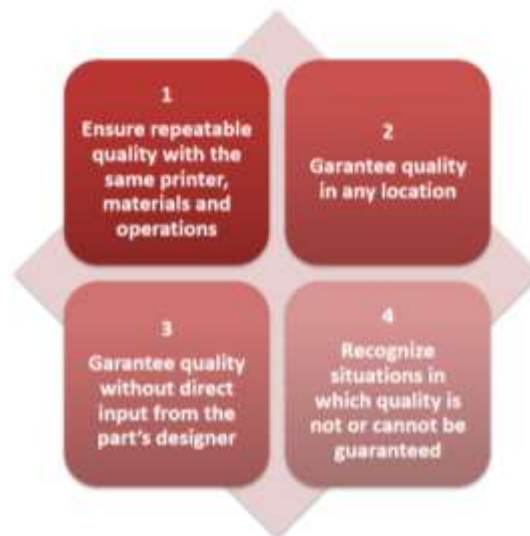
Fig. 6 - Facets of AM technology [34]

The qualification of AM parts demands a different approach from traditional methods, thus, one taking AM processes into account, may offer greater benefits. Therefore, unlocking the full potential of AM may necessitate a reversal of the qualification process to which engineers are accustomed: the development of means to certify AM parts based on design, as well as observations and corrections made during the build process, rather than verifying performance after manufacturing [13, 34].

To address the differences between AM and conventional processes, the science and engineering community is gravitating toward an AM solution centered on three pillars: QA derived from build planning and build monitoring/inspection, linked together with feedback control, as described in table 4 [34].

Table 4 - Key elements of quality assurance in AM [34].

AM Pillar	Description
Build Planning	The use of advanced modeling and simulation to develop a plan machine to produce a specific part.
Build Monitoring	Monitoring with sensors the build process as the part is being constructed.
Feedback Control	Using data from the building monitoring sensors to iteratively update the build planning in real time.

All the strategies available so far, in order to control the process and ultimately achieve a high quality AM product, are presented in Figure 9 [23].

What is possible to say according to the figure is that there are three main methods, being desirable the combination of all of them, i.e., the traditional optimization test, the numerical simulation calculation and the online detection, for a systematic study on the defect formation and control in the LPBF processes. An online detection is conducted for obtaining information on defect morphology, location and dimensions through detection sensors, data processing, image analysis and feedback control. On the other hand, the strategy should also investigate defect formation and evolution mechanisms, including material melt-flow behavior, solidification and shrinkage, the interaction effect of surface tension, capillary force and gravity, by using the numerical simulation method. Finally, combining the information on defect

detection and defect formation mechanisms allows to go further and accomplish the process optimization to achieve the aim of defect suppression and control in an LPBF process [23].
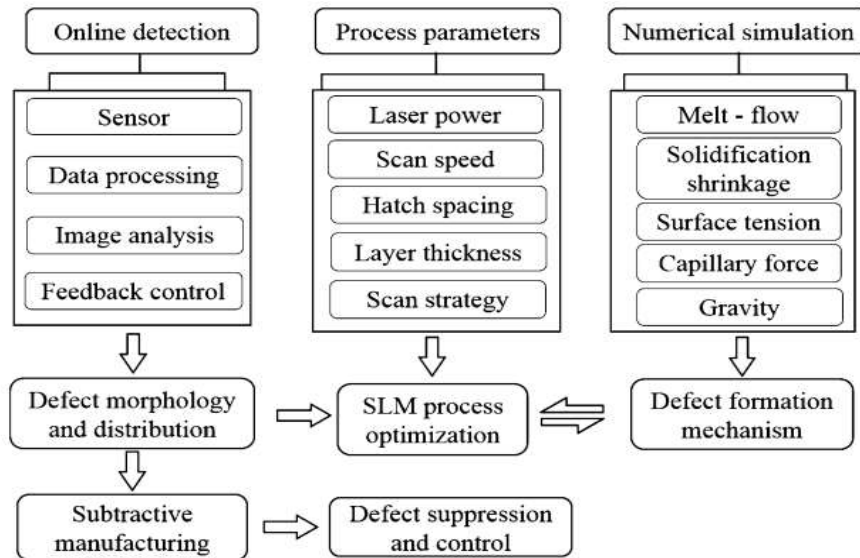
Fig. 7 - Schematic illustration of defect detection and control in an LPBF process [23].

Regarding standards, these are emerging to control several factors that influence AM technology, being available, for instance, standards for destructive and non-destructive evaluation of finished AM parts. Despite these developments, there are no broadly recognized, published standards for the *production* of AM parts. The area is, however, evolving rapidly. The ASTM and ISO together designated a committee to define standards for test methods, design, materials, processes, environment, health and safety, terminology, and potentially file formats. Ideally, these standards will be applicable in the near future across multiple machines and processes, to help maintain consistency in a variety of situations [34, 36].

In order to check if the parts are in accordance with AM standards and client requirements, it's necessary to resort to methods of quality control. That being said, next section, will focus on the techniques available currently.

2.3.1 Quality control methods

In the optimization of processing parameters for AM parts, the measurement of the part densities is essential and of high interest. However, as already been said, there is no common standard. As the interests in several industries are rising, it is essential

to be able to assess the quality of a layer-wise produced part in order to compare the different machines, materials and processes available. The quality of a part contains parameters out of at least three main topics: mechanical parameters (density, mechanical strength, elongation to rupture, fatigue strength), surface quality and dimensional accuracy [37].

Focusing on the density, there are several possibilities for measuring it, being present on table 5. Through OM it's possible to do an analysis of a micrograph of a cross-section of the part, however it is a destructive method and only provides expedited 2D information about the defect. Concerning the SEM analysis, it provides really high resolution images, but it's also a destructive method, much more expensive than OM and requires qualified operators.

Besides, it's important to point out that all these methods are based on specific measurement parameters that affect the result in some degree. An example is the micrograph of a cross-section, where the density is dependent on the magnification and the selection of the cross-section for the micrographs [4, 37, 38].

Table 5 - Destructive and non-destructive methods for porosity measurement [37].

	Archimedes Method	Optical Microscopy	SEM	X-Ray CT	SRiT
Example					
Method	Destructive	Destructive	Destructive	Non-destructive	Destructive
Features	• the simplest method	• widely used method • 2D pore image	• measure shape, size, distribution of very small pores • High resolution	• measure shape, size, distribution of very small pores.	• measure shape, size, distribution of very small pores. • measure in-situ formation of porosity

However, of all these quality control methods, CT offers the advantage of being able to inspect the material structure of the manufactured product in a manner that it doesn't compromise the product's physical integrity. Besides this, it provides the user the possibility to perform dimensional analysis on internal features that are inaccessible by conventional coordinate measuring systems (CMSs) [39].

The X-ray tomography is a class of radiology technic, for which common attribute is the movement of the X-ray. In CT, X-ray radiographs from hundreds of different angles are taken of a sample and contrast comes from differences between the X-ray attenuation characteristics for each kind of material. Mathematical algorithms use this information to reconstruct the interior of the sample and the output is in the form of hundreds or thousands of cross-sectional images, which can be stacked together to form a 3-D image of the sample or part (figure 10) [39, 40].
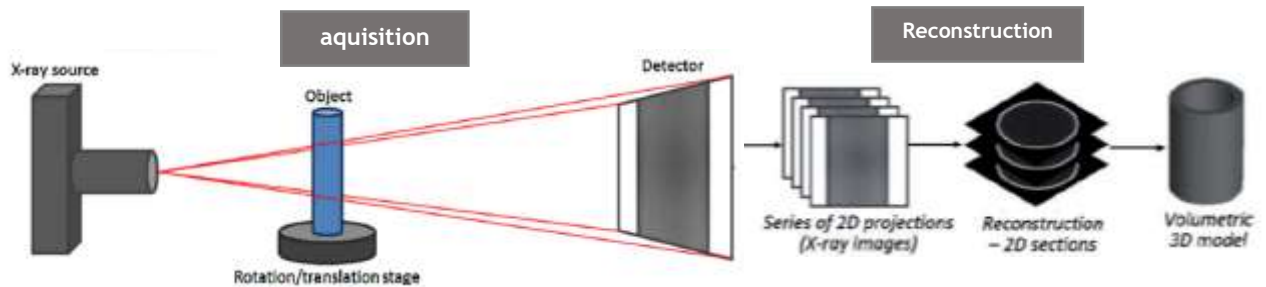
Fig. 8 - Schematic presentation of obtaining data by technical CT [39].

In this way, a map representing 3D geometry, obtained by CT reconstruction, makes it possible to detect hidden material defects inside the reconstructed objects, offering the advantage of doing a quantitative analysis of defects to evaluate total porosity with determination of shape porosity and their spatial distribution. However, CT capacities can go further, as shown in figure 11 three quality checks done with the same CT data: (i) control of form and geometrical deviations (nominal/CAD comparison), (ii) thickness verification and (iii) control of material density/porosity [41-43].
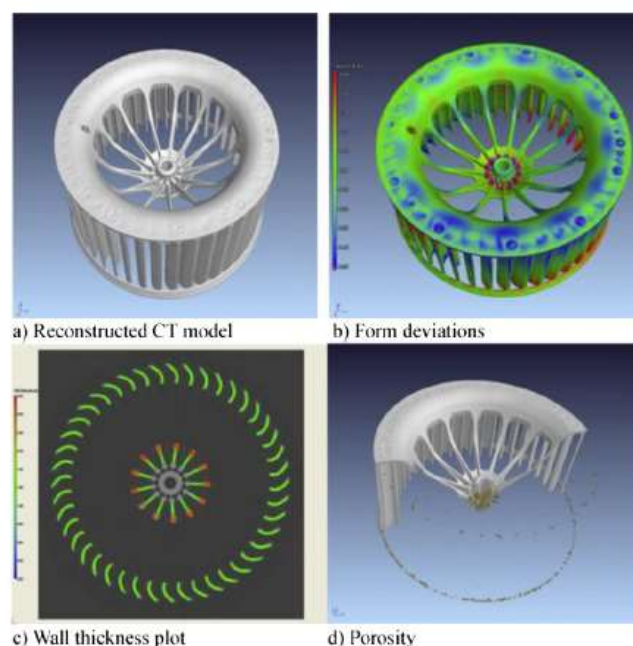
Fig. 9 - CT different quality checks done with the same CT data [41].

On the other hand, there is an uncertainty associated with the CT measurements system as results of several influencing factors, including the influence of the operator because there are several parameters that have to be chosen by the operator. It is possible to point out other limitations, being summarized in figure 12 [44, 45].
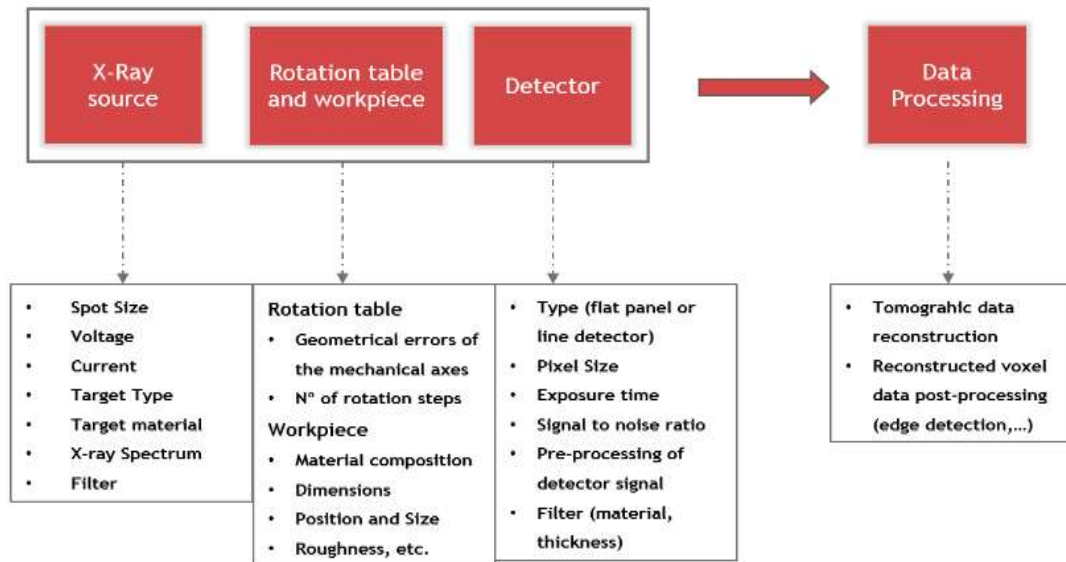
Fig. 10 - Classification of factors influencing the CT performance [44].

All the aspects regarding X-ray source, rotation table and workpiece, detector and data processing can lead to geometrical offsets, misalignments, and instabilities, resulting in reconstruction errors that compromise the quality of coordinate measurements made on industrial CT systems. For instance, it can appear defects associated with artefacts, including beam hardening that is revealed in form of non-homogeneous grey scale recorded for a homogeneous material, or X-ray scattering resulting in significant quality reduction of reconstruction (figure 13) [46].
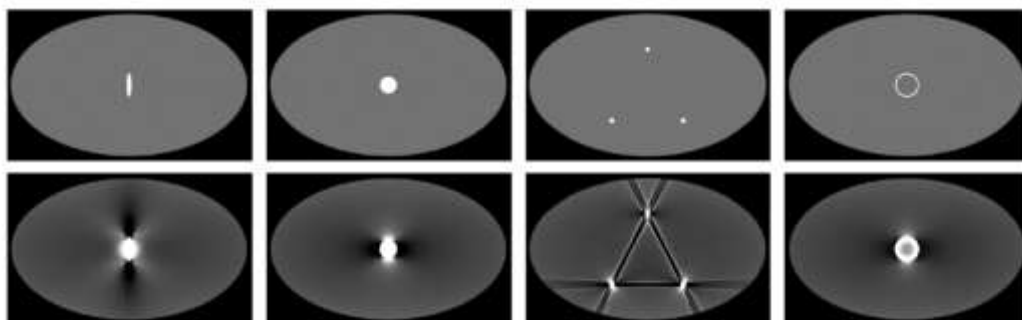
Fig. 11 - Simulated scans without (top row) and with (bottom row) beam hardening, showing that dark streaks occur along the lines of greatest attenuation, and bright streaks occur in other directions [46].

For this reason, it's important that users are provided with a procedure they can use to evaluate the measures of their CT system [46, 47]. However, when compared to CMMs (Coordinate Measuring Machine), which have been on the market for over 50 years, CT as a technique applied for industrial dimensional metrology is relatively new. Procedures and/or standards for the development of a task-specific measurement uncertainty not currently exist. To date, there is a lack of international standards to provide comprehensive procedures and guidelines to deal with the verification of CT systems for dimensional metrology performance. To overcome the lack of international standards for CT dimensional metrology verification, some manufactures have opted to design their own calibration methods. The VDI/VDE 2630 (German guideline for the application of DIN EN ISO 10360 for coordinate measuring machines with CT sensors) is currently considered the only reference document for specification and verification of CT systems used for dimensional metrology and as such is the adopted guideline for several manufacturers, particularly in Europe. It is not an international standard, but it's the only guideline for CT published so far, in this case, by the German body of metrology. Ultimately, manufactures must develop detailed maintenance and calibration plans for equipment, representing this an important competitive advantage [46, 47].

3. Experimental procedures

In this chapter are presented the methods that were adopted for the accomplishment of this project, being made, a detailed analysis to the equipment and mode of operation. The following flowchart is presented in order to explain in a succinct and lucid way the steps taken throughout the project (figure 14).
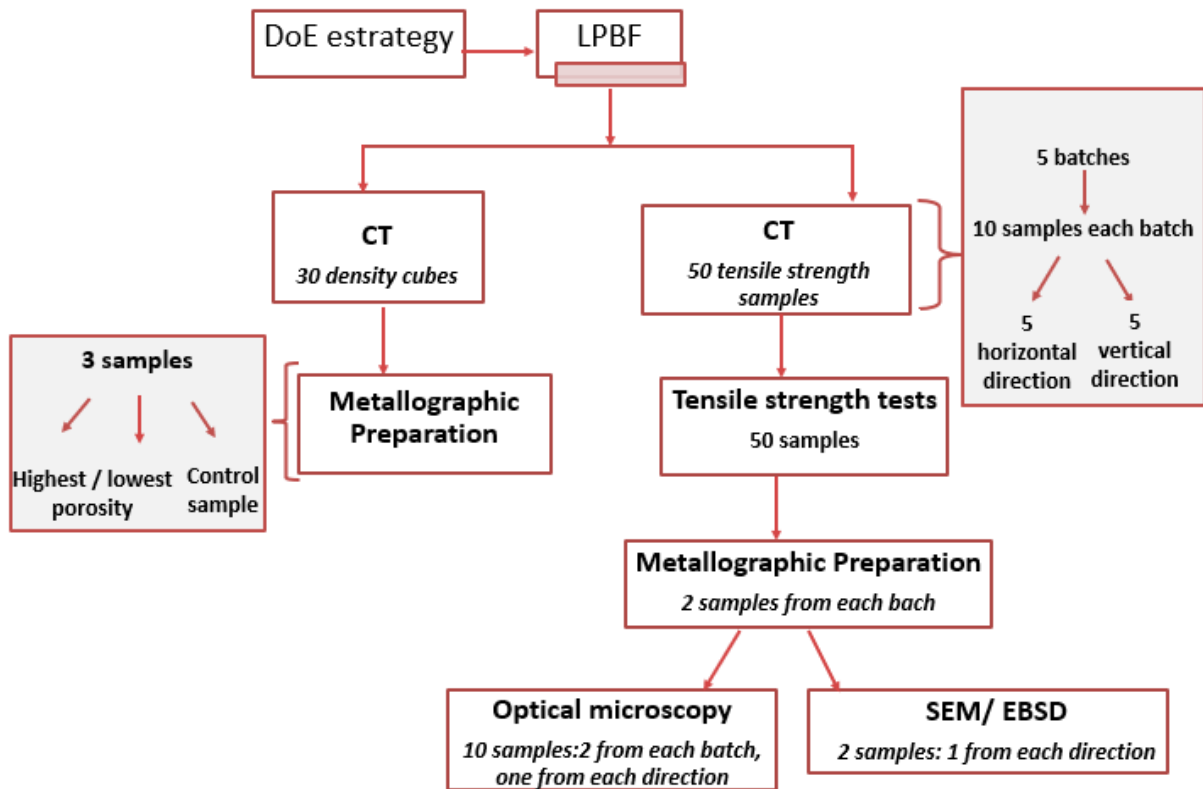
Fig. 12 - Experimental procedure flowchart.

The DoE strategy for the selection of LPBF parameters where made in a previous work develop by Christoph Wilsnack [48]. The parameters and the strategy were chosen based on Design of Experiences method, namely, A Box-Wilson Central Composite Design, commonly called 'a central composite design'. This method consists in a full factorial and partial factorial designs to which the central point and the star points are added (figure 15). The star points represent new extreme values (low and high) for each factor in the design. Annex A presents a more detailed information on this method.
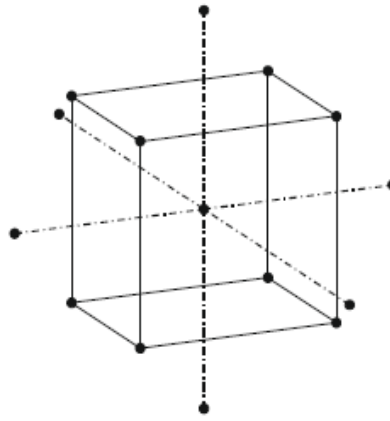
Fig. 13 - Central Composite Design representation.

In this way, to determine the maximum density, a statistical design with the four factors is set up. These factors are independent of each other and thus suitable for setting up a test plan. This extends a test room with the variation of the factors on five levels and ensures a good estimation of the target density. The central point is represented by the existing parameter set in table 6. The star points are arranged with the magnification factor a = 2 around the central point, in order to ensure the rotation of the system with four factors (annex A). The statistical validation of the experiments is carried out by repeating the central point.

Table 6 - Given parameter set from Renishaw [48].
-

Laser Powe in Js^{-1}	*Hatch* distance *in* μm	Point distance in μm	Exposure time in μs	d$_{layer}$ in μm	Scan strategy
150	100	60	100	30	10 mm strips, 67 ° rotation

The equipment adopt for the research was an AM250 machine by Renishaw and their specifications are presented in table 7 [48]. The powder used has a density of 8,19 g / cm^3 and a melting temperature of 1260-1336 °C. The powder composition is presented in table 8 and its characteristics are displayed in table 9 [48].

Table 7 - Renishaw AM 250 Specifications [48].

Property	Specification
Laser	Ytterbium-Faserlaser (λ=1070 nm)
Maximum laser power	200 W
Laser beam diameter	70 µm powder surface
Installation space	245 x 245 x 300 mm3
Layer thicknesses	20 – 100 µm
Panel heating	70 – 170 ˚C

Table 8 - Composition of the examined powder [48].

Element	Ni	Cr	Nb	Mo	Ti	Al	Co	Si	Mn	Fe
%	51,43	20,12	5,27	2,76	1,17	0,54	0,83	0,13	0,35	17,4

Table 9 - Powder properties [48].

Quality Features	Measured Parameter
particle shape	spherical
Particle surface	smooth
satellite particles	occasionally recognizable
Inner porosity	barely recognizable
Particle size distribution	$20 < d_{Particle} < 45$ µm
Max. Particle size	45 µm
Min. Particle size	10 µm
Moisture content of powder	0,034 ±0,009 %

In order to manufacture the cubes for the density study the dimensions and geometry presented in figure 16 were considered. A total of 31 cubes were produced, 24 specimens plus 7 equal control specimens in order to ensure the study reliability. The process parameters set for the Inconel 718 cubes are displayed in table 10.
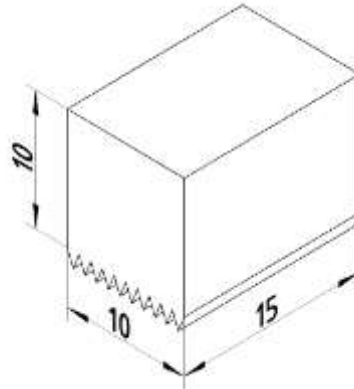
Fig. 14 - samples geometry and dimensions.

Table - 10 - Cubic samples process parameters.

number	P_{laser} in J s-1	d_{hatch} in µm	d_{point} in µm	$t_{exposure}$ in µs
1	125	70	40	70
2	175	70	40	70
3	125	130	40	70
4	175	130	40	70
5	125	70	80	70
6	175	70	80	70
7	125	130	80	70
8	175	130	80	130
9	125	70	40	130
10	175	70	40	130
11	125	130	40	130
12	175	130	40	130
13	125	70	80	130
14	175	70	80	130
15	125	130	80	130
16	175	130	80	100
17	100	100	60	100
18	200	100	60	100
19	150	40	60	100
20	150	160	60	100
21	150	100	20	100
22	150	100	100	100
23	150	100	60	40
24	150	100	60	160
0-1	150	100	60	100
0-2	150	100	60	100
0-3	150	100	60	100
0-4	150	100	60	100
0-5	150	100	60	100
0-6	150	100	60	100
0-7	150	100	60	100

The round tensile test specimens were produce according to ISO 6892-4:2015 with a diameter M10 (figure 17) [49]. Overall under study were 50 tensile strength specimens, divided in five batches numbered as 0 (control batch), 1, 2, 3, 4. In each batch the first five samples were produced in the vertical way and the last five samples on the horizontal direction. Table 11 presents corresponding process parameters for each batch.
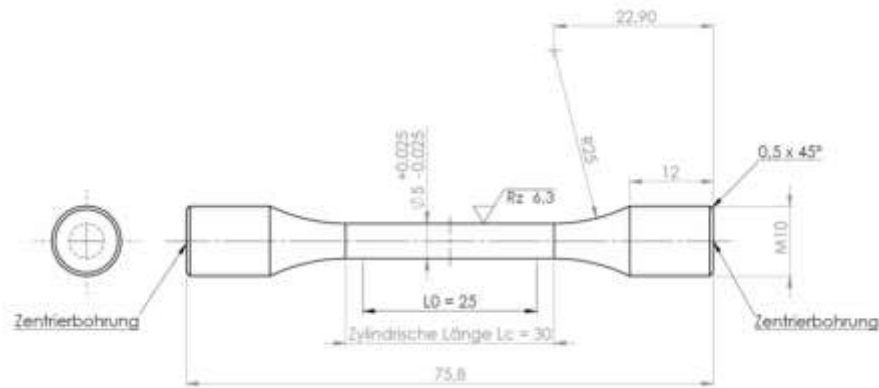
Fig. 15 - Geometry and dimensions of the samples [48].

Table 11 - Tensile strength specimens' process parameters according to each batch.

number	P_{laser} in J s-1	d_{hatch} in µm	d_{point} in µm	$t_{exposure}$ in µs
0	150	100	60	100
1	100,00	60,31	33,63	114,58
2	200,00	79,00	64,00	97,00
3	127,00	95,00	44,00	118,00
4	100,00	105,00	47,00	106,00

3.1 Characterization Techniques

In order to evaluated the cubes and tensile strength specimens different characterization techniques were used. As displayed in figure 14:

The density cubes were analyzed using the CT in order to obtained the porosity value and defects morphology according to each set of process parameters. The OM technique was used to obtain the porosity value in a specific cross section and then compare with the CT results.

The tensile strength specimens were also analyzed using the CT in order to obtain the porosity percentage. After that, tensile tests were executed in order to obtain data concerning the mechanical properties, namely, UTS (ultimate tensile strength) and ductility according to the building direction and process parameters. For the microstructure evaluation, OM and SEM/EBSD techniques were used to identify the differences between the building directions.

The methodology adopted in this research as well as the description of the techniques used is presented below.

3.1.1 Computer tomography (CT)

From all the CT abilities, in this research this technique was used predominantly for porosity analysis, concerning its distribution, sphericity and to determine the ratio between the parts volume and defect volume. In order to achieve satisfying results in the CT it's crucial to take several steps into consideration. Figure 18 shows the main steps taken during the analysis of the specimens under study, namely thirty one density cubes and fifty tensile strength specimens.
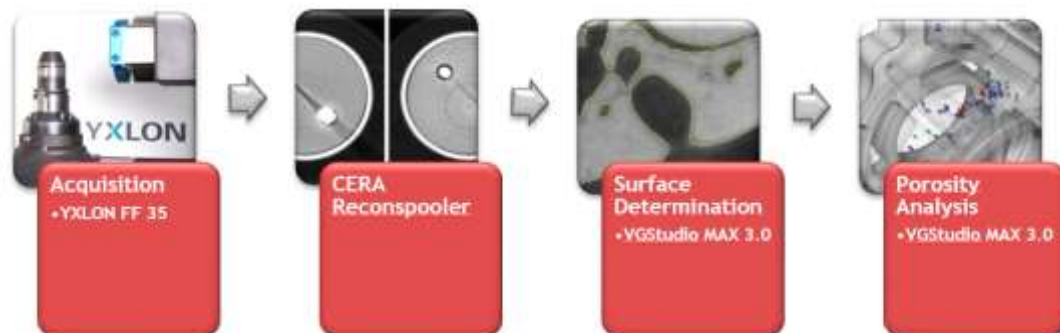
Fig. 16 - Steps performed on the CT analysis with focus on the machine and software used.

The first phase is possible using the YXLON FF 35 machine and the process begins, with the right positioning of the part inside the CT's chamber, in a way that all the surface is projected on to the detector but with minimum travel path of the X-rays through the part. Figure 19 a) and b) shows how the density cubes and the tensile strength specimens were positioned in the specimens holder. In this study, all the analysis were made using a filter, namely, 1 mm brass filter.
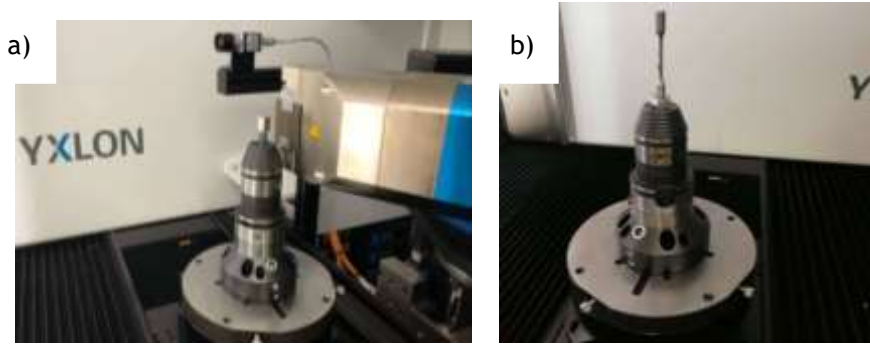
Fig. 17 - a) Positioning of the cubic samples and (b) tensile strength specimens.

The next step includes selecting the intelliguard option and then defined several parameters, related to: tube (voltage, current intensity), detector (frame rate), manipulator (i.e. focus detector distance (FOD), focus detector distance (FDD)), etc. All the settings for the density cubes and tensile strength samples are presented table 12.

Table 12 - Cube and tensile samples CT parameters.

Sample	Part Position	Tube				Detector		Manipulator					Helix Scan	
		Voltage (kV)	Amperage (µA)	Filter material	Thickness (mm)	Frame rate (Hz)	X	FOD	FDD	Velocity Factor	Number of projections per turn	Frames per projection	Skip Frames	Geometry Calibration Scan
Density Cubes	Vertical	150	150	brass	1	2	0	35	700	0,5	360	1	0	on
Tensile Strength Samples	Vertical	150	150	brass	0,5	1,5	0	35	1100	0,5	400	1	0	on

Regarding the YXLON reconspooler software, this corresponds to the last stage of the scanning phase. This software supports a broad range of cone-beam and fan-beam CT applications, that include, image pre-processing such us bad-pixel correction, intensity correction, and median filtering. Herewith, it's possible to adjust several parameters using YXLON reconspooler, annex B shows all of parameters with the related definition. In this work it was selected bad pixel reduction, noise reduction in *Projection Space* and *Volume Space*. These parameters were kept the same for all of the samples.

The software VGStudio MAX was used to determine the surface and to make porosity analysis. This software is the world's most advanced software platform for industrial CT data analysis and visualization. During the specimens analysis, three functions of the VGStudio MAX 3.0 were used, namely, *Registration*, *Surface Determination* and *Porosity Analysis*. For this research it was chosen the *Simple registration* mode. To perform the surface determination, it was used the option *Advanced Surface Determination* in the software, in order to define material boundary by locally adapted gray values. Figure 20, shows the preview of the surface determination with advance mode.
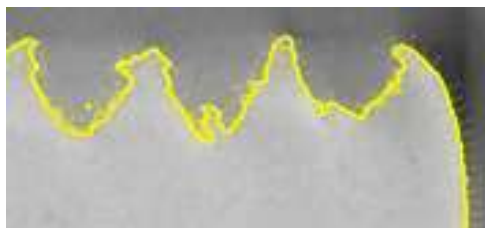
Fig. 18 - Detail of the advance surface determination of an object corner with different gray values.

The final step consists on doing the Porosity/Inclusion Analysis module and this option includes various algorithms to investigate voxel data sets for internal imperfections such as voids and contaminations. Annex C shows highlighted in red the fields important for porosity analysis and annex D shows the settings selected.

3.1.2 Tensile Strength Tests

In order to evaluate specimens mechanical properties and obtain the stress-strain curves, tensile tests were performed. This tests were executed using a MTS systems corporation machine and were performed based on EN10002-1-2001 standard. In this

way, after being measured the diameter of all the fifty samples, they were tested with a velocity of 2 mm/min at room temperature. The assembly necessary for carrying out the test is shown in figure 21. The data processing was made using Excel software.
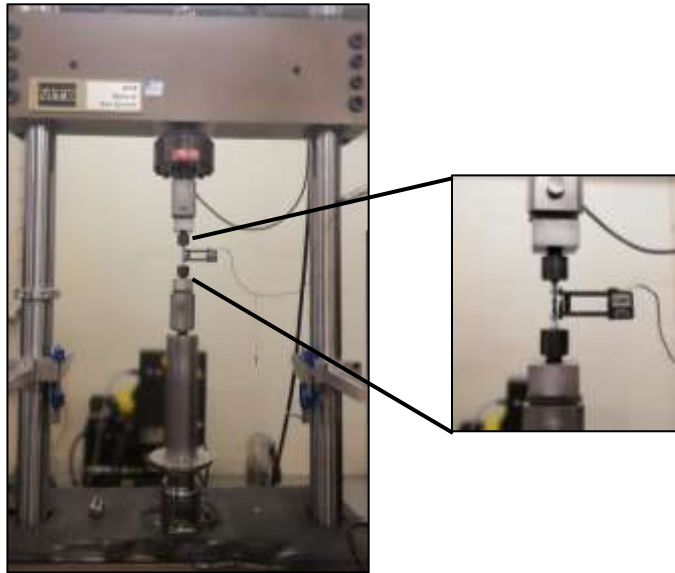
Fig. 19 - Tensile Strength Test machine used with the specimen positioned.

3.1.3 Microstructural Analysis by OM and SEM/EBSD analysis

The microestructure evaluation and porosity quantification by OM and SEM/EBSD analysis required a metallography preparation.

The metallographic preparation for all the specimens annalised consisted in several steps: cutting, mouting, griding and polishing. For microstructure evaluation by OM an additional step was made: etching. All the specimens were cut with the discotom machine by Struers and after cleaning were embedded with hot mounting acrylic resin with a heating time of 2 min and a cooling time of 11 min. The pressure and temperature were, respectivily, 275 bar and 180°C. This stage was performed in a SimpliMet 1000 machine.

The grinding step was performed with the sequence of 320-400-600-1000 grit using a polishing machine with 300 rpm and water on. For polishing it was used 4000-grit and a 0,1 μm diamond suspension, both with 150 rpm. The polishing step ended using a 0,1 μm silicon suspension.

Talking about the strategy used for the density cubes, the samples with highest and lowest porosity value and one control sample were observed in the optical microscope without etching, just to quantify the porosity present in one cross-section. In order to have confident results, the entire surface of the sample was run having analyzed approximately thirt fields with an ampliation of 5x. The OM analysis was made manually, meaning that there may be areas that have been analyzed twice or areas that have not been analyzed. The OM software in question is Las Leica sofware and for the porosity quantification it was used the *phase analysis* module. Lastly, the same cross-section was chosen in the CT making it possible to compare the two techniques (figure 22).
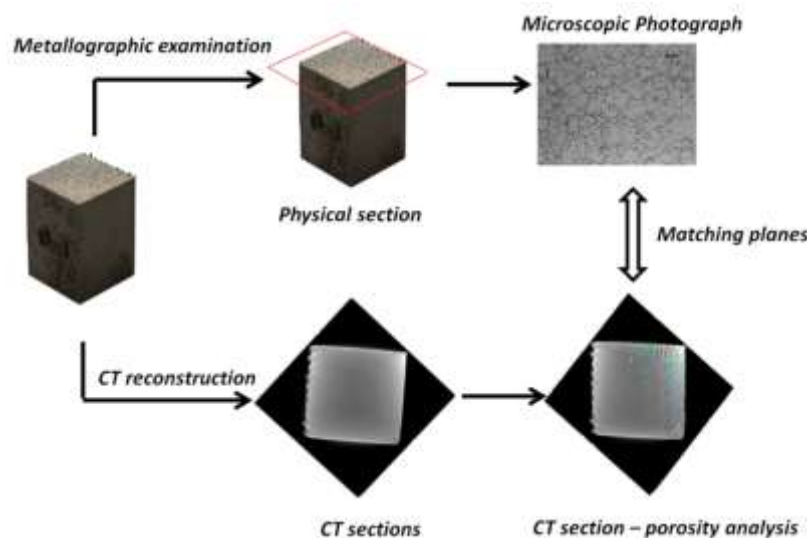
Fig. 20 - Flowchart that represents the strategy used for the density cubes.

For microstructure evaluation, it was chosen two samples of each tensile strength samples batch, one from the vertical and horizontal direction, giving a total of ten. After that, cuts were made in the mooring heads of the samples, considering that it was an area that suffered very small plastic deformation. In order to reveal the microstructure it was executed an etching with waterless Kalling's reagent composed by 100 ml of C_2H_6O, 100 ml HCl and 5 g of $CuCl_2$ with an exposure time of 30 seconds. In order to obtain the images of the microstructure, it was used the OM software mentioned above.

SEM/EBSD analysis were performed in two tensile strength samples (one vertical and horizontal direction) from the control batch (number 0). The equipment used was the FEI Quanta 400F Scanning Electron Microscope and the TSL OIM Analysis software was used for the data processing.

4. Results and Discussion

Firstly, in this chapter are presented the evaluation of density cubes by CT and their comparison with porosity quantification by OM and with Arquimedes method. It is also analyzed the influence of the process parameters in these characteristics. Secondly, tensile strength tests were performed in all tensile strength specimens in order to study the influence of process parameters in mechanical porperties. Complementary techniques, namely CT, OM and SEM/EBSD, were used to understand the correlation between microstruture and porosity with mechanical properties.

4.1 Density Cubes

Figure 23 shows how the results of density cubes are presented. In this way, initially it will be made a comparison between the CT results and other techniques, namely, OM and Archimedes method. In the first case, the comparison doesn't concern just the porosity value but also includes the distribution and sphericity along a specific cross-section. This first part, aims to evaluate the CT's accuracy and reliability.

The second branch has the objective of perceiving the influence of the process parameters on the porosity parts/specimens. With this, initially the relationship between the porosity evaluated by CT and the energy density is established graphically. Afterwards, it's presented the interaction plots made with Minitab software for a further analysis of the effect of porosity percentage on the individual and simultaneously process parameters.
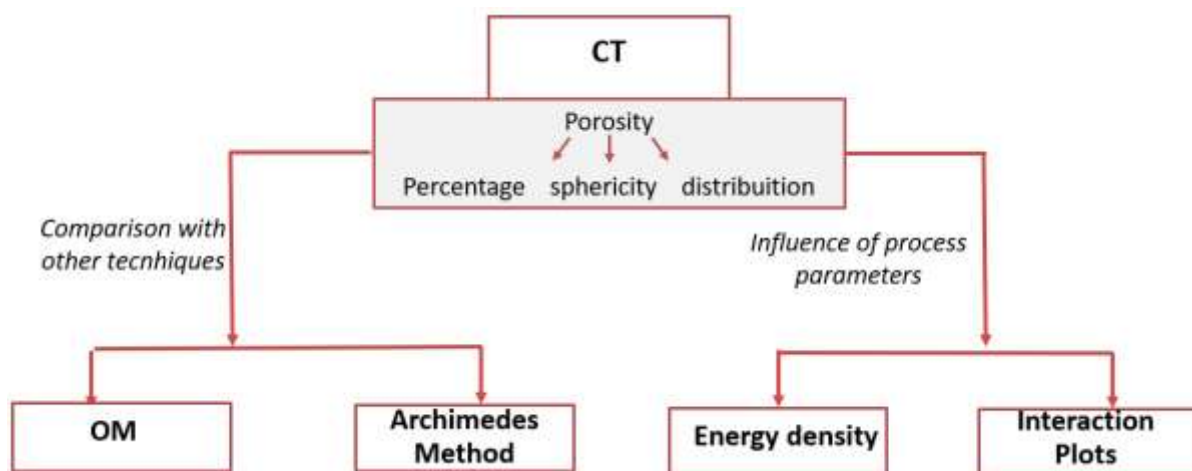
Fig. 23 – Flowchart concerning the density cubes results.

Thusly, figure 24 shows the porosity evaluated by CT for each specimen of density cubes produced. It should be noted that the values of porosity present are the ratio between material volume (mm^3) and defect volume (mm^3).
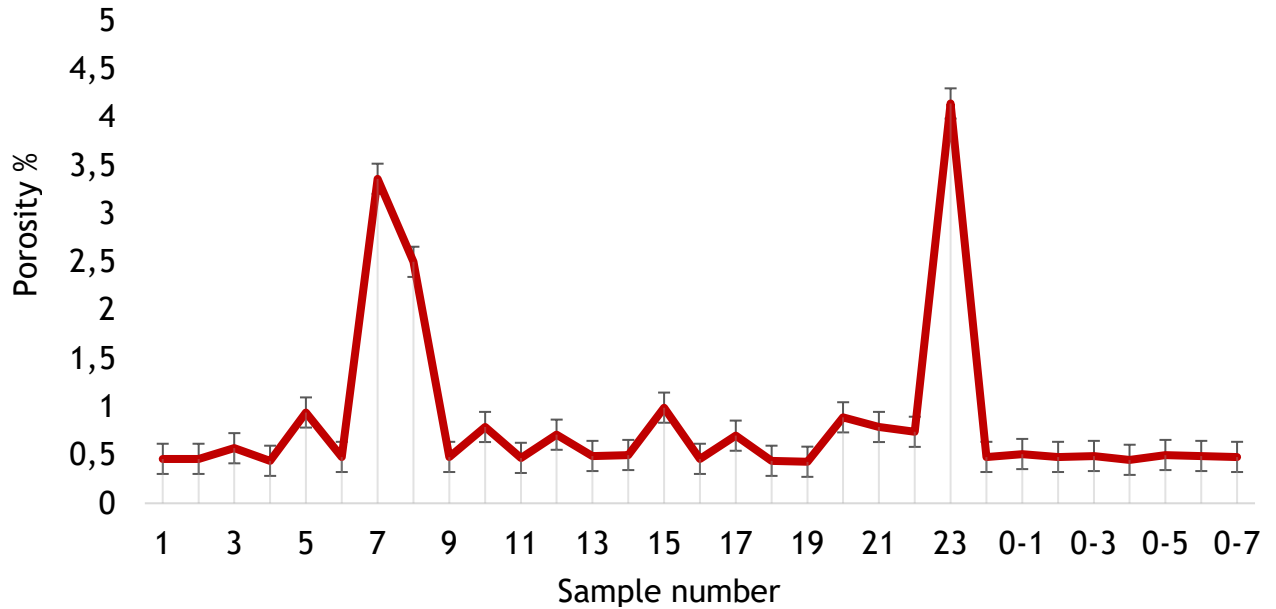
Fig. 22 - Results concerning porosity given by CT.

According to these results, the specimen that presents the highest porosity value is specimen number 23 (4.13% ± 0.37) and the lowest is specimen number 19 (0.43% ± 0.30). Therefore, is pertinent to compare these specimens with one of the control specimens, for instance, specimen 0-1 . In figure 25, it's displayed the CT results concerning the porosity percentage.
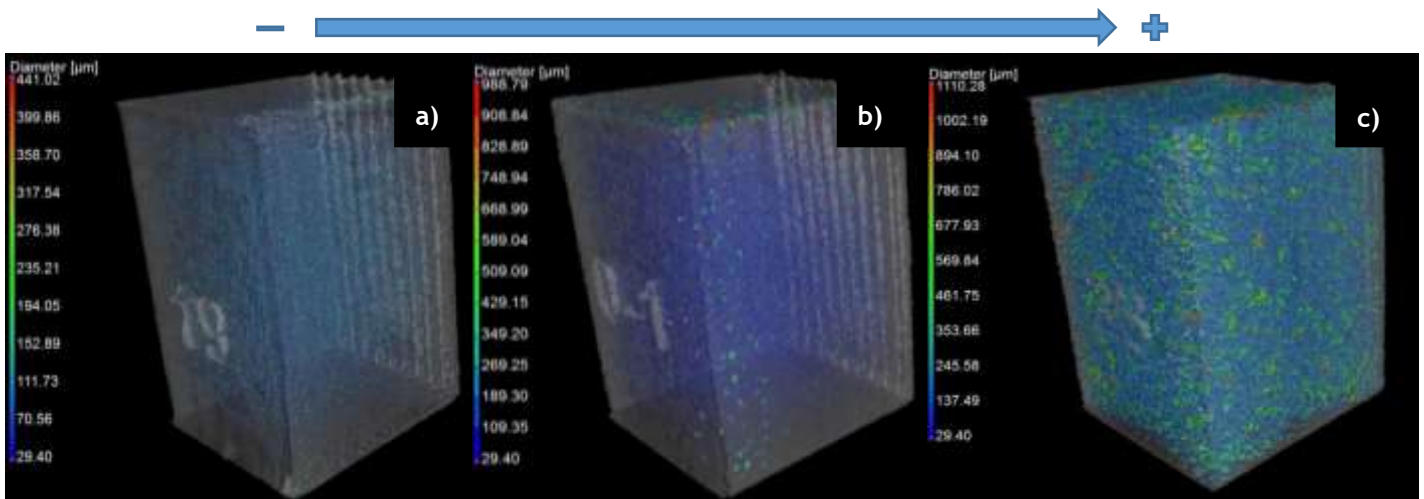
Fig. 23 - 3D CT results concerning porosity on samples number 19, 0-1 and 23.

The disparity of the results of the specimen 23 in comparison with the other two, comes from the fact that the process parameters have exerted a great influence. The specimens 19 and 23 have the same LP and PD, namely, 150 J.s^{-1} and 60 µm, herewith, the difference comes from the DH and ET applied. While specimen 19 uses a DH of 40 µm and ET of 100 µs, specimen 23 uses 100 µm and 40 µs. Applying such a high value of DH in specimen 23, may lead to porosity between layers, not assuring an overlapping between two layers in a row. Besides, the ET of this specimen is the lowest compared to all the specimens, showing apparently, that this value could be the reason for such a high porosity formation, implying that this time is not enough to promote the particles' melting. The study developed by Z. Zhou [50] proves through SEM images that a low ET leads to discontinuous melted laser scanning tracks.

Specimen 19 and the control sample 0-1 have exactly the same parameters with the exception of DH, 40 and 100 µm respectively. Specimen 19 shows the lowest porosity due to the short DH, proving that applying a reduced DH is advantageous in a way that this generates an overlapping of two adjacent lines of molten metal, avoiding the appearance of porosity.

Figure 26 presents the CT results, but this time, focusing on sphericity, being this, the measure of how closely the shape of an object approaches to a mathematically perfect sphere. From its analysis, it's possible to observe that specimen 19 and 0-1 present similar results, showing sphericity around 0.70-0.90. The last specimen, presents lower values of sphericity, namely, around 0.40-0.70, characteristic of the green and blue scale colors. This means that specimen 23 presents defects that are not close to the spherical shape, and with this, the morphology of its defects will be discussed down below trough OM images.
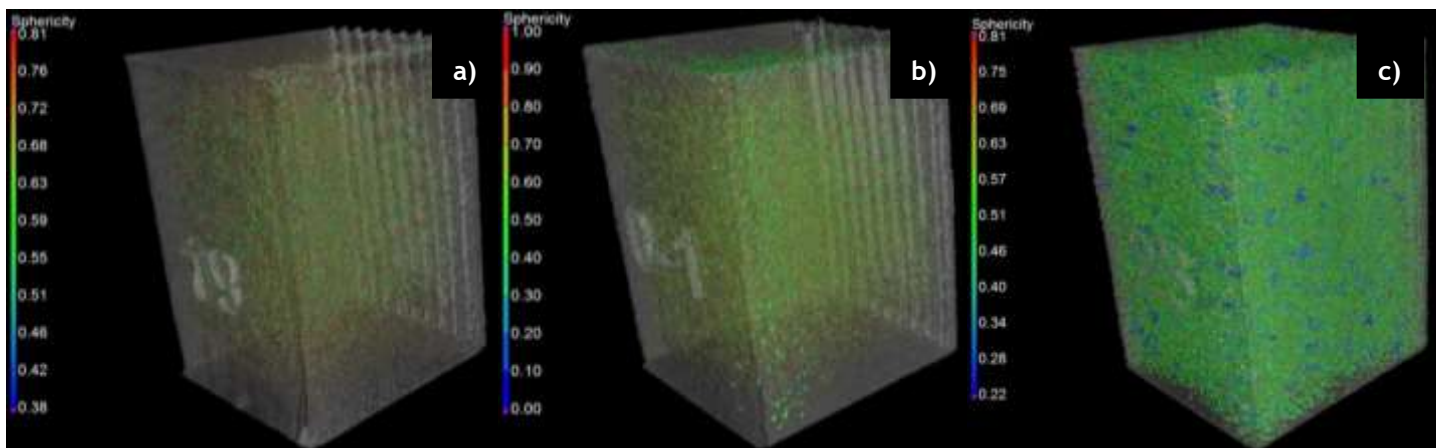
Fig. 24 - CT results concerning sphericity on samples number 19, 0-1 and 23.

After analyzing a specific cross-section in the OM, it's possible to find the same cross section in the CT and compare one field of observation. That being said, figure 27 illustrates this comparison between the cross sections through images (CT images vs OM images).

a)   b)

c)   d)

e)   f)
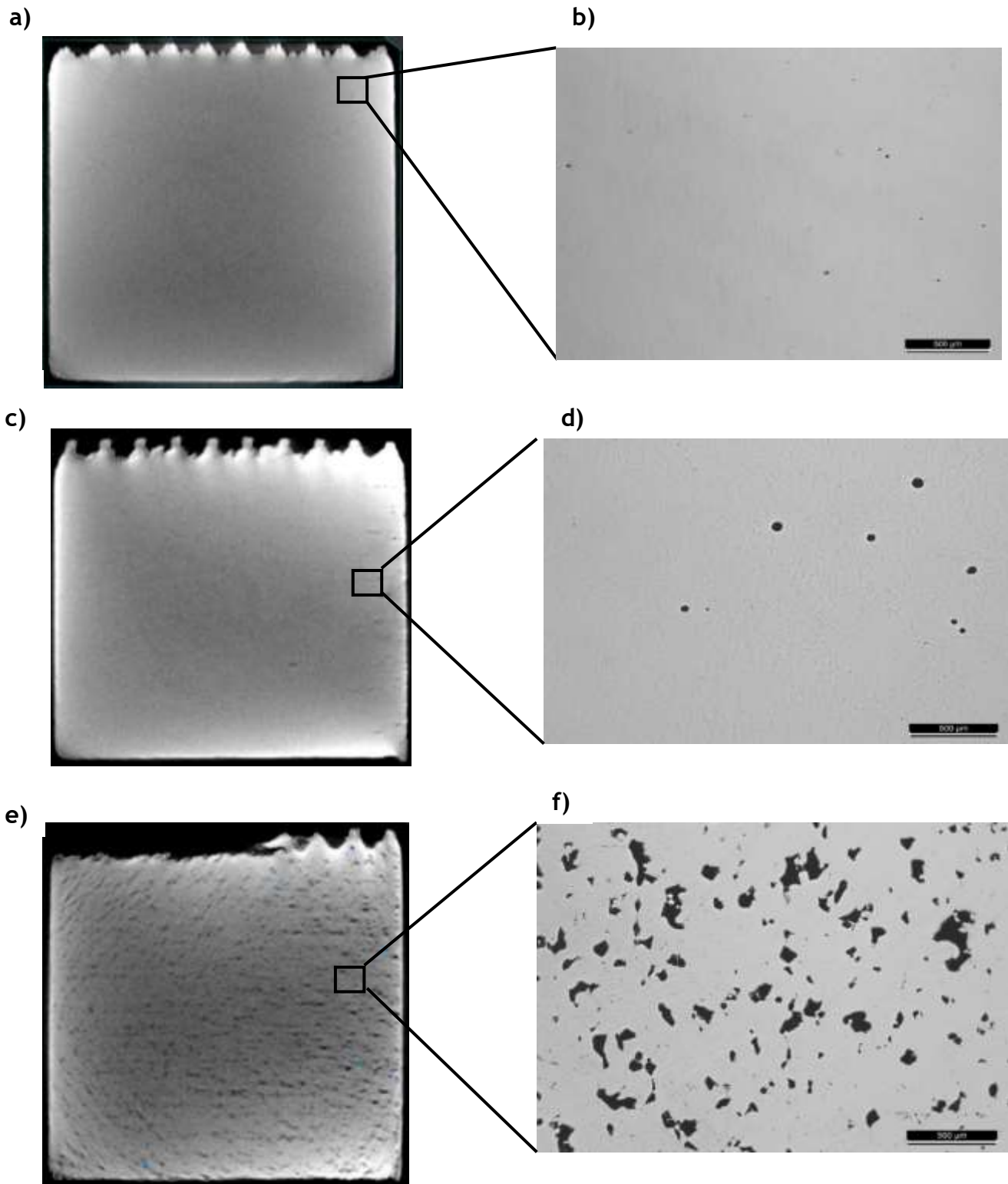
Fig. 25 - Comparison between the same cross section evaluated by CT and OM in samples 19 (a) (b), 0-1 (c) (d) and 23 (e) (f).

Making a detailed analysis of these images, it's possible to indicate that they are in agreement, in the sense that the porosity observed in each section corresponds in the two techniques and it's growing along the specimens under study. Besides, comparing the OM images with the morphology analysis made by CT (figure 26), we noticed that there is also a coherence, since the specimens 19 and 0-1 show a porosity with an approximately spherical morphology and specimen 23 shows another type of morphology, namely, angular, flat defects and voids, resulting in a lower sphericity percentage.

Focusing on the type of porosity, namely, near-spherical defects like in specimens 19 and 0-1, these are related to surface roughness, particle melting, melt pool stability and re-solidification mechanisms, as has also been described by Mumtaz [51, 52]. This kind of porosity, also suggests that the gas present in the starting powder layer became trapped in the melt pool, thereby producing residual porosity in the solidified bulks. Based on the study by XinZhou [50, 51], the macroporosity presented by specimen 23 could be a consequence of, insufficient energy that gives unmelted spots in the laser scanned tracks due to reduction in the size of melt pool and leads to the formation of voids along or between the lines of the hatch pattern.

For a further comparison between the two methods, table 13 presents the data given by the software of both techniques. Both OM and CT porosity values concerns the defect area in the cross-section (ratio between the analyzed area and the defects area), allowing a more reliable comparison. Herewith, the differences between the two methods are not significant, and it's important to keep in mind that both techniques have an uncertainty associated. For instance, both methods are influence by the operator, and in this way, the software parameters chosen may change according to the person that is responsible for the analysis.

Table 13 - Comparison of porosity value of CT and OM techniques concerning the samples 19, 0-1 and 23 for the cross-section.

Sample number	19	0-1	23
OM	0.20 ± 0.24	0.58 ± 0.21	$10,97 \pm 3.40$
CT	0.31 ± 0.25	0.42 ± 0.33	12.00 ± 2.13

Overall, although the results are similar, CT offers the possibility of doing a volumetric observation, allowing a 3D perception of the defects. Besides, it doesn't require any kind of preparation and it's a non-destructive method, being this an incredibly important asset in the AM field, considering that often only one piece is produced it's not advantageous to damage during QC. The fact that it is a non-destructive method is an advantage that other methods cannot match, since it's often to be produced single parts or very small series it's important to maintain the integrity of the parts during quality control. The disadvantage of this method is that although no metallographic preparation is required each analysis takes a significant amount of time.

Until now, CT was compared to the OM in order to compare results concerning the porosity morphology and percentage. However, considering that one of the main goals of this research is evaluate CT's measurements accuracy, it's relevant to correlate its results with another common method, namely, the Archimedes method. The values of this last technique are provided by C. Wilsnack master thesis [48] (figure 28).
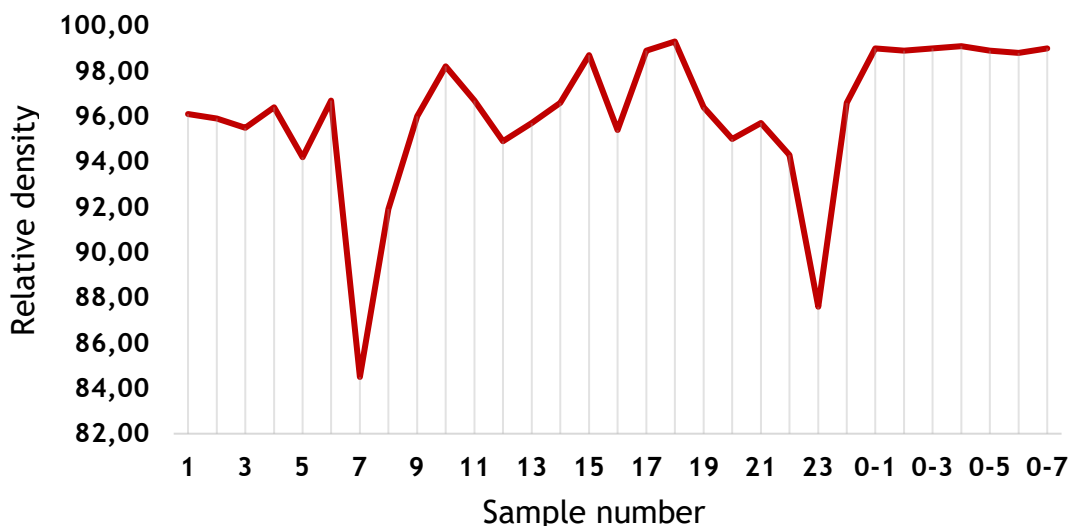
Fig. 26 - Values concerning the relative density for each sample [47].

The graph that relates the porosity given by the CT and relative density is presented on figure 29. First, a regression fit equation was added being this the "best fit" line for the data, in other words, an average of where all the points line up. In this case,

it's represented a linear regression, the line is a perfectly straight showing a linear relationship between the methods under study.

Further on, the points highlighted in red represent the control specimens, showing a relative density between 98.9-99.1% that corresponds, according to the CT, to a porosity of 0.45-0.50%. The points highlighted in light blue reveal that the relative density increases with the porosity and this not a coherent fact, although the CT analysis was repeated in these specimens. These incoherent facts don't have a clear explanation, but it's a known fact that these measurements may be a consequence of several factors during the production cycle phase and in quality control, being both dependent on the operators influence.
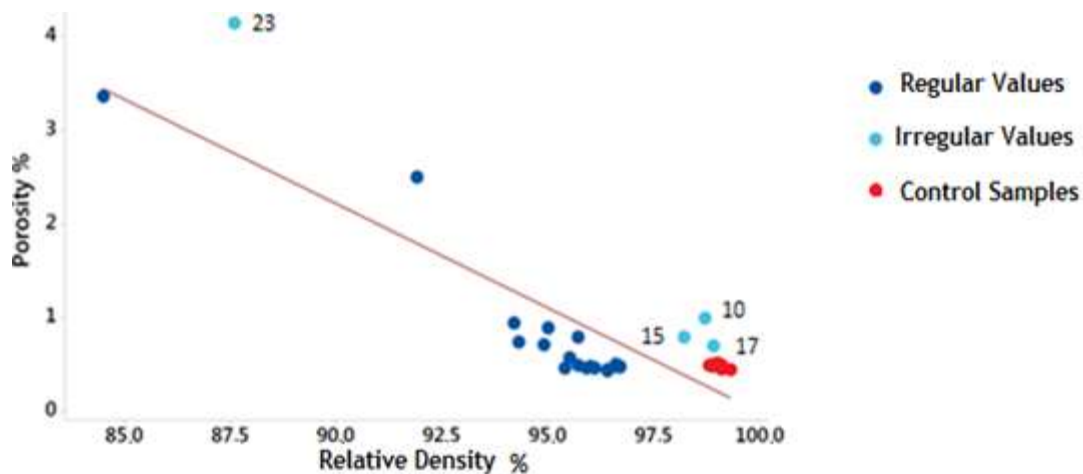
Fig. 27 - Graphic representation of Porosity vs Relative Density-

Evaluating the CT's performing what it's possible to say is that in such a small batch there are some deviations, being normal to rise some questions respecting its accuracy and reliability. Nonetheless, it should be point out that most of the specimens under study have different process parameters and these leads to difficulties to access its accuracy. In this way, it would be more expedite to evaluate the CT measurements when all the samples have the same process parameters because in this scenario, the porosity expected should be all the same and in case of nonconformities it would be immediate consider an inaccurate technique. Taking this into account, focusing on the control samples (red points) that have same parameters, when analyzing the CT's outcome regarding this samples, it is pretty satisfying because the porosity values barely changes.

Lastly, although there are still many concerns related to the CT, this technique is constantly subject to improvement actions. With this, it's expected that its uncertainty will become better over time being more and more an asset in the AM field.

4.1.2 Energy density

During the literature review, the concept of energy density was introduced and through the parameters involved in this study it's possible to make the proper calculations (figure 30).
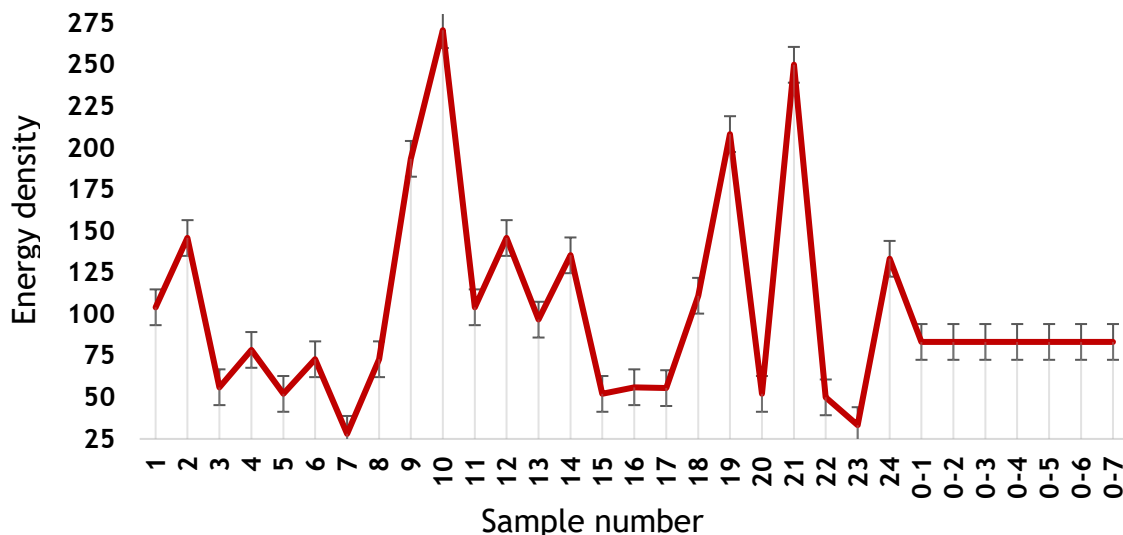
Fig. 28 - Results concerning the energy density for each specimen.

With the ED density results it's possible to make a correlation with the porosity given by CT (figure 31). With this, applying an ED less than 50 J.mm^{-3} the specimens show higher porosity levels. This means that applying a very low ED, the energy is not enough to promote the total melting of the powder particle and as consequence the defects amount increases leading to higher porosity percentages.

From an energy density of 52 J.mm^{-3} the values are approximately constant, around 0.49% porosity, except for point highlighted (specimen number 8). Although these specimens have a high value of ED, the PD (80 μm) and DH (130 μm) provoked a higher porosity percentage probably since the distance between layers and between the laser points is elevated, originating porosity between layers and in the same layer.

At higher energy densities, there isn't a considerable amount of pores on the part due to melting of the powder mixture by the laser beam and this leads to less porosity percentage. However, even when providing a higher amount of ED, for instance above 200 J.mm^{-3}, it doesn't mean that the porosity level decreases, on the other hand, it is the same or slightly higher.

Checking the results corresponding to the graph of porosity vs ED with other studies [53], it is verified that the curve presented is in agreement and shows a satisfying outcome. Overall, it's evident that the formation of a porous structure can be controlled by manipulating the amount of energy provided to the system.
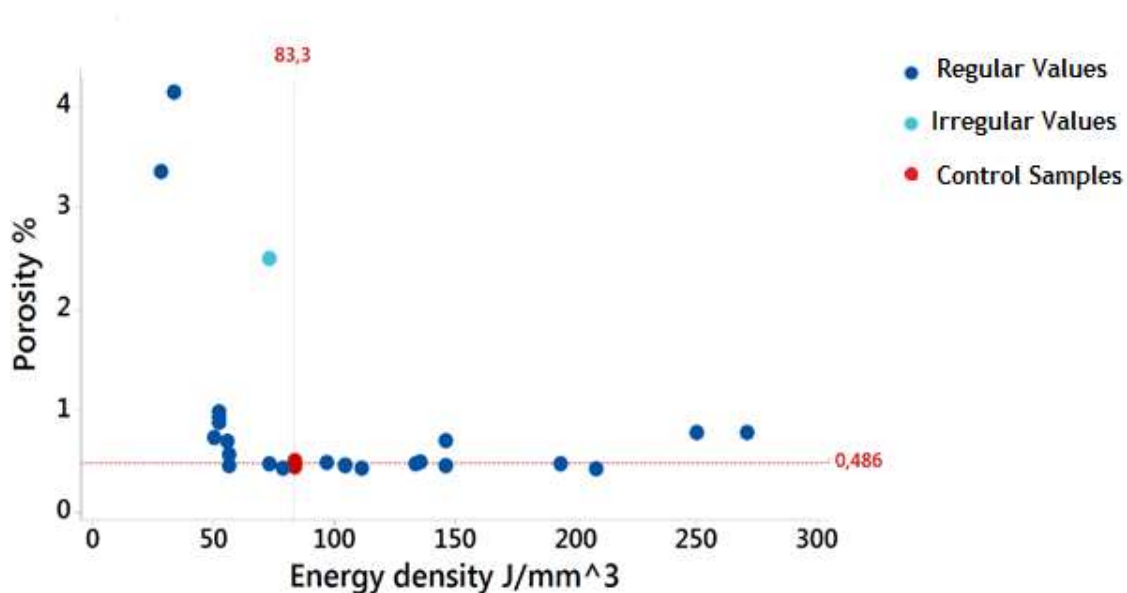
Fig. 29 - Graphic representation of Porosity vs ED.

In figure 32 the graphic shows the correlation between relative density and ED and through its analysis, the relative density increases with the applied ED until 83.3 J.mm^{-3}. From this value forward the relative density values are approximately constant even applying a higher ED. The value of specimen highlighted in light blue is the same as figure 31, result of the explanation given above.

The results of the two graphs are in agreement considering that the information provided is complementary, when the porosity decreases the relative density increases, what was expected.
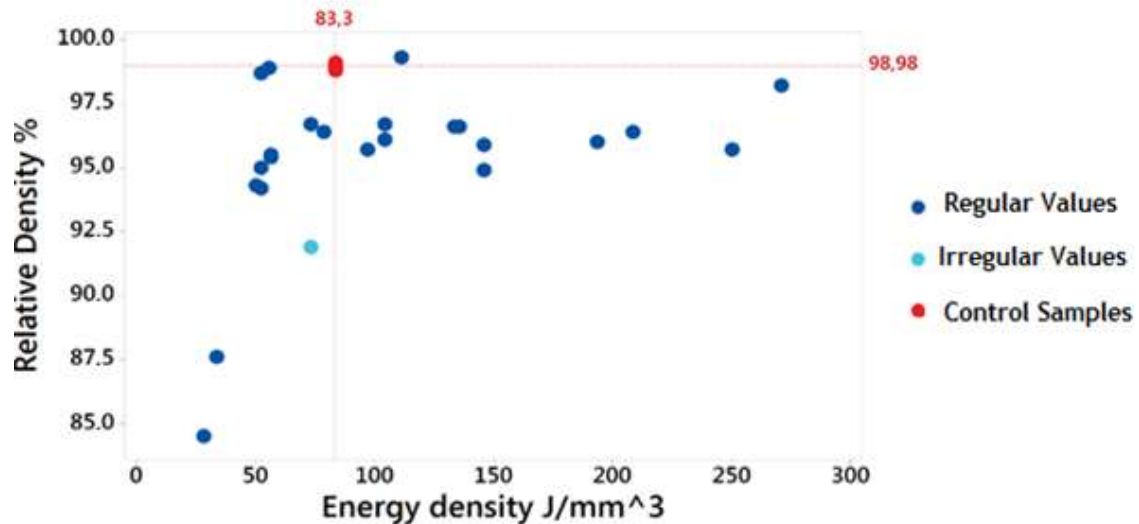
Fig. 30 - Graphic representation of Relative density vs ED.

4.1.3 Process Parameters Interaction

In figure 33, it's presented the effects that each parameter has on the porosity value through a main effects screener, provided by one of the minitab's functions.

Through its analysis it should be noted that in general all values are close to the mean except for the application of an ET of 40 µm, resulting this value in the greatest deviation from the average, considering all points. This implies that this exposure time is not sufficient to cause total melting of the particles and therefore, the amount of pores and other defects are much higher in this case.

The variation of the LP values doesn't have a significant effect on the porosity values because all the points are close to the average, being the interval from 100-200 J.s^{-1}, a reasonable interval. In this way, the LP parameter has the least isolated effect on porosity.

The PD and DH of 40 µm results in the lowest porosity value in the specimens. And this makes sense considering that a DH of 40 µm allows the developing of two overlapped layers, reducing the probability of porosity appearing between two layers.

The ideal parameters setting combines a LP of 200 J.s^{-1}, PD of 40 μm, ET of 160 μs and DH of 40 μm. For a more detailed information about the main effects on porosity, see annex E.
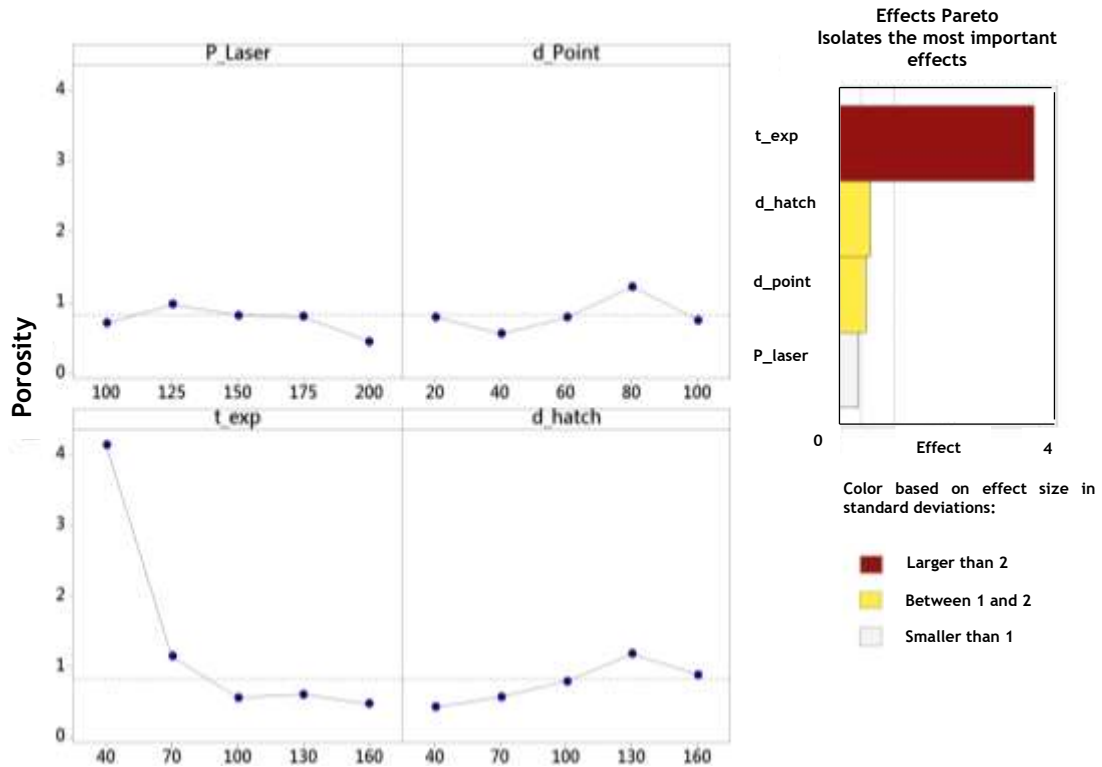
Fig. 31 - *Main effects of process parameters on Porosity.*

Although the main effects analysis is useful to verify that the chosen parameter amplitude produces variation in the porosity, this is a very individual approach. Besides, it's known that during the process the effects of the parameters are not independent, so it's relevant to take a look at the interaction of all the parameters simultaneously. In this way, the diagram presented in figure 34 illustrates the interaction between all the parameters. The Interaction Plot is used to show how the relationship between one categorical factor and a continuous response depends on the value of the second categorical factor.

Evaluating the lines is essential to understand how the interactions affect the relationship between the factors and their response. In this case the diagram is composed mainly of nonparallel lines, this means, that an interaction occurs and the more nonparallel the lines are, the greater the strength of the interaction.

In the case of LP, represented in the first line of the diagram, it's possible to observe that for all the five values chosen for LP there is an interaction with DH at 100 µm, PD at 60 µm and ET at 100 µs. It's possible to recognize that there is an area where the five lines are approximate, this means, that the interaction between LP and the other factors is strong, and the porosity obtained is a product of the interaction of several factors and not of an isolated factor. The same is true for the other lines in the diagram because no window has parallel lines.

All the windows, instead of having a connecting line between several points, apparent just a point, for instance, LP of 200 J.s⁻¹ (grey and triangle symbol). In this type of cases, it's difficult to make an analysis of the influence of the application of a particular factor, since there is only one specimen subject to this condition. The ideal, would be to have several samples with the same process condition in order to obtain a line in the diagram and check if there would be more interaction with other lines.
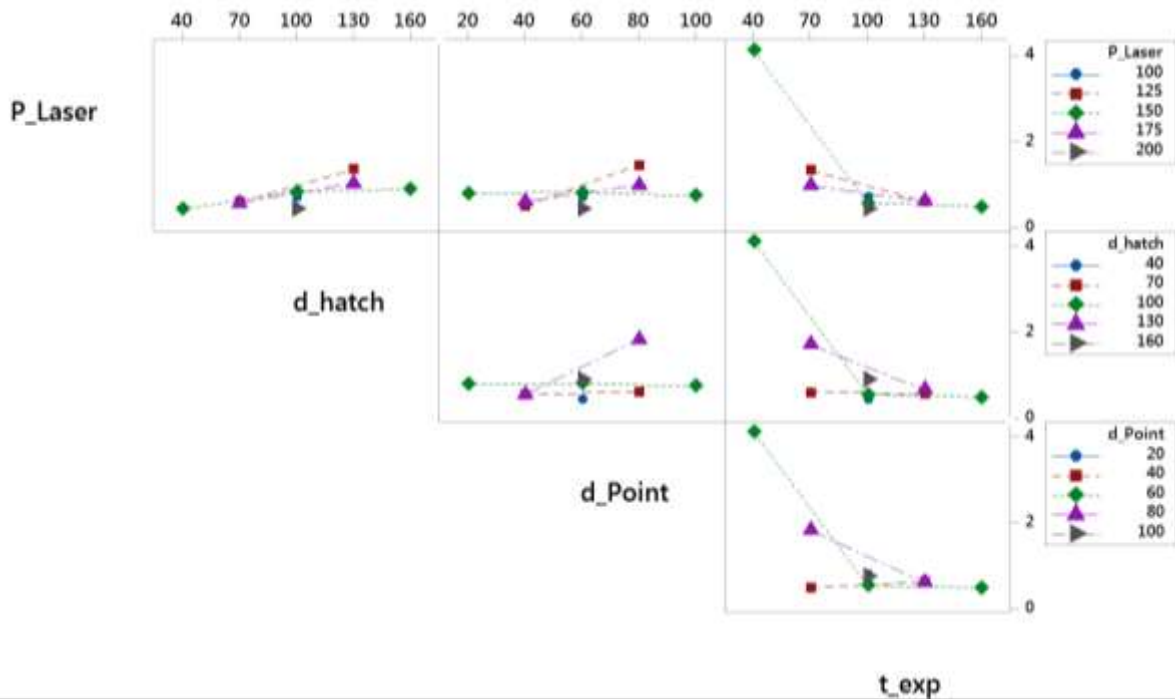
Fig. 32 - Interaction plot for porosity %.

4.2 Tensile Strength Specimens

This section will provide all the results concerning the tensile strength specimens and figure 35 shows the techniques used in these speciemens along with the main purpose of each. In this way, this analysis begins with the presentation of the tensile test results. From here, complementary techniques, namely CT, OM and SEM/EBSD, were used to understand the influence of process parameters and building direction (XY and Z) on porosity and mechanical properties.
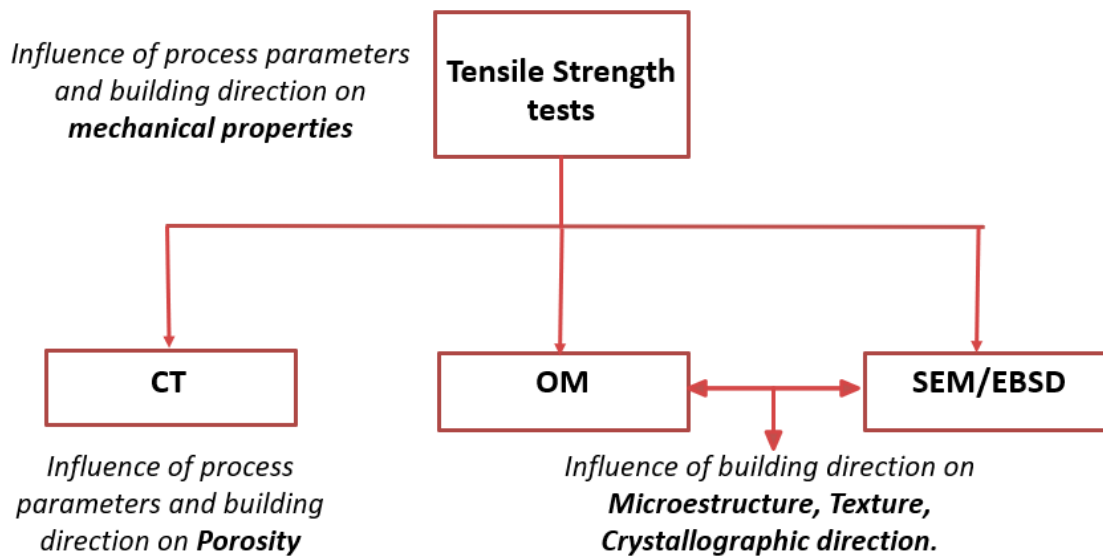
Fig. 33 - Flowchart concerning the Tensile Specimens results.

Regarding the tensile tests, the tension-strain curves were obtained by the average of all the results in the horizontal direction (HoD) and vertical direction (VD) is presented on figure 36 a) and b). These curves enlighten the fact that the parts built in the VD show a lower ultimate tensile strength (UTS) and as consequence present a higher strain value. The inverse is verified in the parts manufactured in the HoD, higher UTS but reduced ductility. The differences in the strain value is almost 10%, making a considerable aspect to take into account for some applications. In this way the average UTS and strain for the VD is 925±149 MPa and 28±8 %, and for the HoD is 1036±206 MPa e 17±6 %. The reason for such a high deviation in UTS is related to the fact that it is an average of all batches, agglomerating specimens with different process conditions.
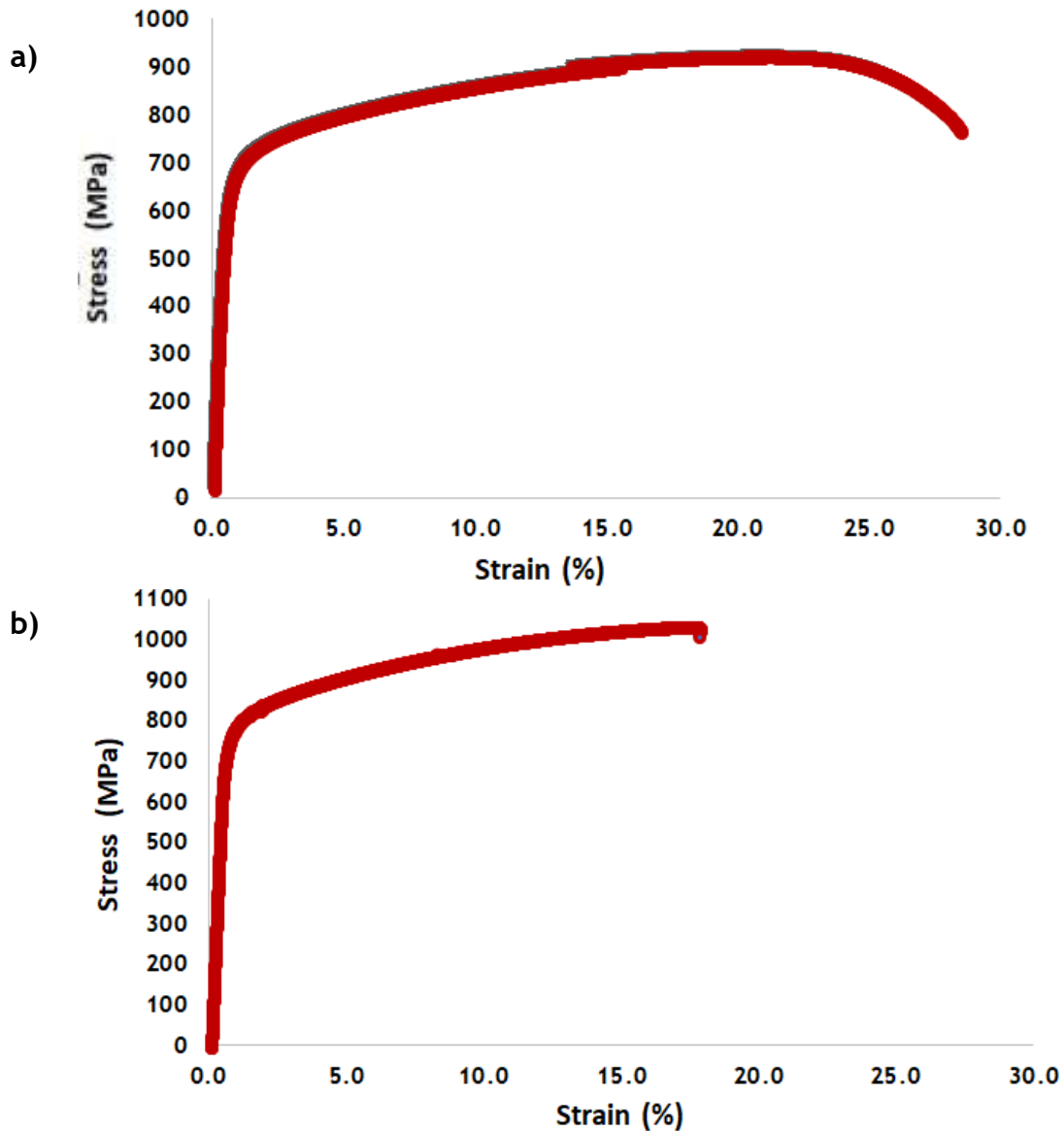
Fig. 34 - Tension-Strain curves for the vertical (a) and horizontal (b) samples orientation.

Moreover, the type of fracture present for both directions is also different, the samples built in the VD showed a «cone-cup » fracture, typical of a plastic deformation fracture. On the other hand, the samples built in the HoD present a fracture typical from elastic deformation or a mix fracture from plastic and elastic deformation. Besides, some of the lowest strain values coincide with rupture in the gage length limit, probably this aspect could be a consequence of concentration points at the surface (surface roughness) and the fracture mechanism started from that region.

For a more detailed information, figure 37 presents the results concerning the UTS for each batch, differentiated each direction (HoD and VD). Through its analysis it's possible to check that in every batch, the UTS is higher in the HoD than in VD. The VD in batch 1 and 2 presents the lower values of UTS and the HoD of batches 0, 3 and 4 the higher values of UTS.
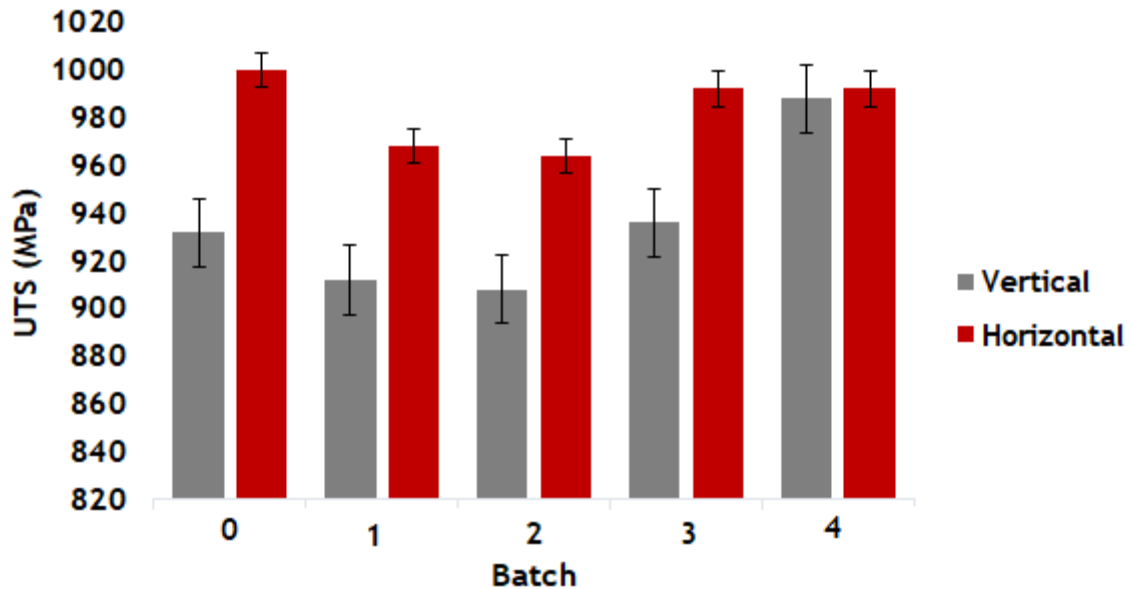
Fig. 35 - Graphic representation of UTS in each batch, VD and HoD.

However, in figure 38 that presents the results concerning the strain, it's possible to see that the samples with lower values of UTS display a higher strain value and the same relationship is verified in the samples with higher UTS. In this case, the VD shows a higher strain value in every batch.
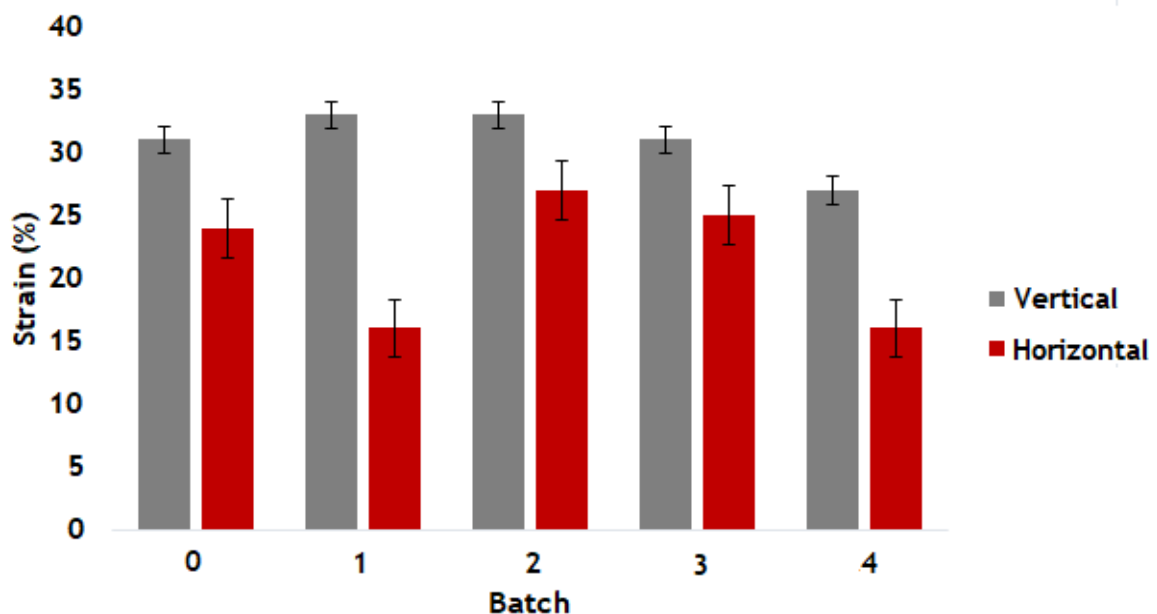
Fig. 36 - Graphic representation of Strain in each batch, VD and HoD.

Regarding the relationship between mechanical properties and process parameters it's possible to say that the different parameters did not exert a drastic influence on the mechanical properties, when considering the same building direction in every batch. In another words, the UTS and ductility values do not present a significant disparity when looking at the same building direction. This can be explained by the fact that the values of the process parameters are similar and it is not possible to observe a greater disparity. However, when looking at the same batch, built under the same process parameters, there is a greater disparity in the vertical and horizontal directions. The effects of build direction and orientation on mechanical properties remain unanswered. Some works report that the orientation has no clear effect on UTS or yield stress but influences the elongation [54, 55]. The differences in the grain growth orientation may promote variations when the tensile tension is applied in the samples. In this way, the influence of the crystallographic direction will be addressed later when presenting the results of SEM/EBSD and OM.

According to a study developed by S. Gorsse *et* al. [54] another theory for the anisotropy in the HoD and VD is related to the porosity. If the defects are perpendicular to the loading direction, the defects are expected to open at relatively low stress levels. If the defects are parallel to the tensile loading axis, the opening of these defects becomes more difficult. It is worth noting that size, morphology and nature of porosities also influence the mechanical properties. With this, is pertinent to complement the results of tensile tests with the porosity values given by CT and try to come up with a relationship between the two techniques (figure 39).
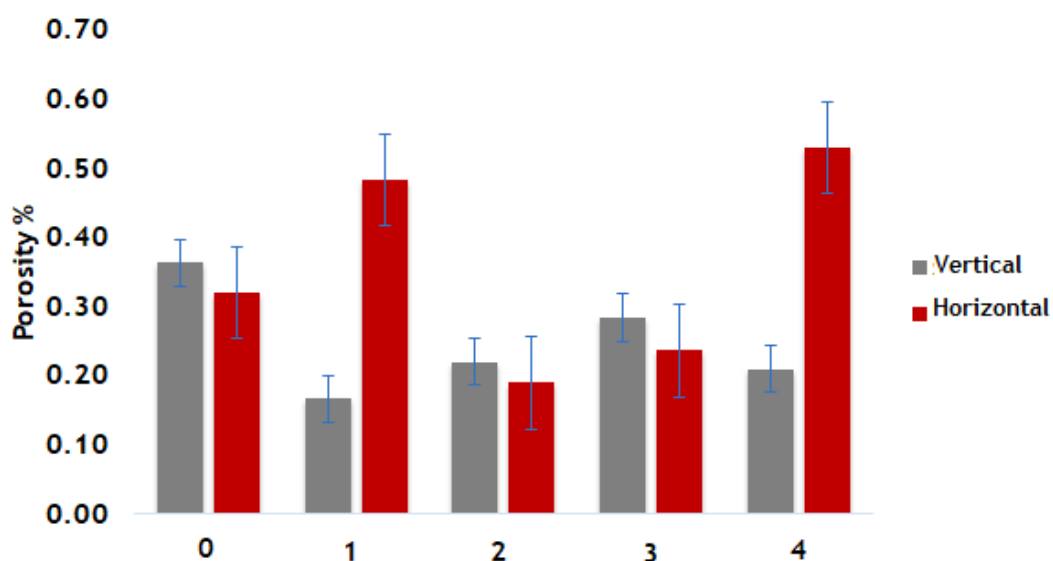
Fig. 37 - CT porosity values concerning the tensile strength samples.

What it's possible to observe in figure 39 is that although in the CT results, batch 1 and 4 had a considerable amount of porosity in the HoD, this porosity didn't have severe consequences with respect to UTS, not showing a decreased value. In the same sense, although the batch 1 in the VD has shown little porosity, the value of UTS is relatively low in comparison with the remaining conditions. However, when it comes to strain values, the highest's porosity values leads to a low ductility and, for instance, the low porosity shown in the batch 1 VD led to a high strain value. In this way, the presence of porosity affects negatively the strain value, meaning that high porosity results in low strain value. In this sense, the presence of different defects (i.e. flat defects and angular) that can form inside a layer or between layers, will affect mechanical properties, specially ductility. Defects like pores tend to act like tension concentrating points which hinder the movement of displacements and this will have repercussion in the deformation mechanism during the tensile tests, leading in most cases to higher UTS.

Besides this relationship what is interesting to see is that the porosity in the HoD of batch 1 and 4 is significantly high and what these batches have in common is the low value of laser power applied (100 J.s^{-1}). Figure 40 displays the specimens according to the building orientation, alongside with the layer length. The laser path is way shorter in the VD and this promotes a lower thermal gradient, meaning that when there is the formation of the next layer, the re-melting of the previous layer is efficient because the temperature has not dropped significantly. This leads to less porosity, due to a good interlayer connection, avoiding the appearance of pores or defects between layers. The opposite occurs in the HoD, because the laser path is much longer, there may be areas where the powder doesn't re-melt totally due to the lowering of temperature, leading to higher values of porosity.

a)   b)
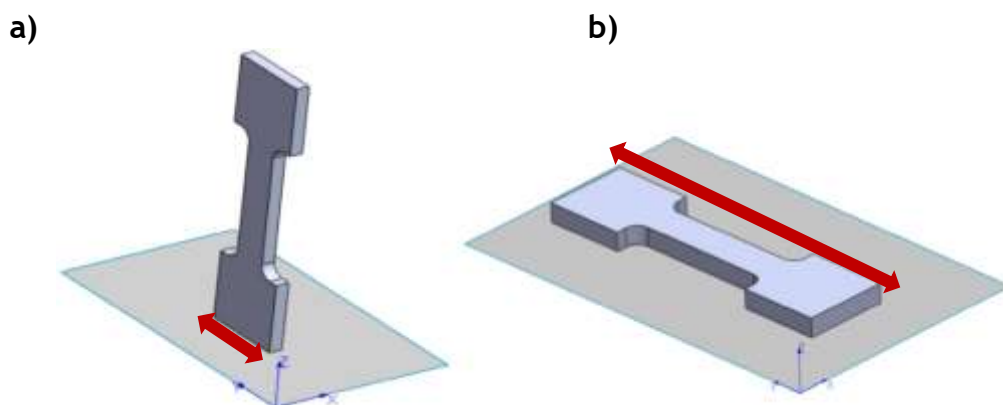
Fig. 38 - Schematic representation of tensile strength specimens and the layer length in each building direction: VD (a) and HoD (b).

Overall, there is anisotropy of mechanical properties of samples manufactured parallel and perpendicular according to the main platform of LPBF system. Both the mechanical properties and porosity depend on building direction, the laser path and the thermal gradients involved. This effect of anisotropy may be decreased by heat treatment (stress relief, stable microstructure, and phase composition) and HIP (closing internal defects such as pores and cracks). High residual stresses during LPBF is one of the limitations of this technology and, for solving of this problem, it should be used special strategies of hatching (for example, "chessboard hatching") and carefully prepared support structures.

So far, what can be stated is that the LPBF process has a directional effect on the properties of the forming parts due to its basic deposition principle. However, in order to understand why this change occur and for that purpose it's important to analyze in detail the results obtained from the OM and SEM/EBSD.

The OM images selected correspond to the control batch (number 0) and are presented as an example since the remaining batches presented similar characteristics. Through its observation (figure 41) it's possible to realize straight away, that the etching wasn't that efficient when it comes to reveal the microstructure, grain morphology and phase constituents simultaneously. That being said, it was necessary to find a balance between revealing the grain boundaries and the laser path without appearing to be over etched. For both directions it's possible to see an overview of the layer structure of horizontal and vertical specimens with the distinct melt pool boundaries. Gas pores are evident in the specimens, and some of them are near or on the layer boundaries, being possible to see, for instance, in figure 41-b. For vertical specimens, the microstructures reflect the laser melt pools that appear predominantly half-cylindrical shape. Besides, the spacing between the melt pools is close to the hatch space, based on the measures made by the Image J software. This kind of structure is common to appear during LPBF parts analysis, being referenced in [1, 56]. Besides, in figure 41-b with more magnification it's possible to see that areas, especially near, the melting pool boundary, present fine cellular-dendrite microstructure. The melt pools are not necessarily symmetrical and are not identical to each other. What it's known is that the Laves phase embeds in the interdendritic region, and by the alignment of Laves phase the growth directions of the cellular-dendrites are stablished. It is also visible in figure 41-b that the

growth directions of cellular-dendrites are not perfectly parallel to the building direction, but instead tilted some degrees away from the building direction. A study developed by D. Deng *et* al [32] also displays this dendritic structure of Inconel 718 parts produced by LPBF. In the horizontal specimens, the melt pool boundaries have a different shape, showing a cross-hatching scan strategy. It's possible to see some grain in the bigger magnification figure (41-d), however it's not enough to do a full characterization. Here de dendritic structure is not perfectly clearly, making it hard to extract information.
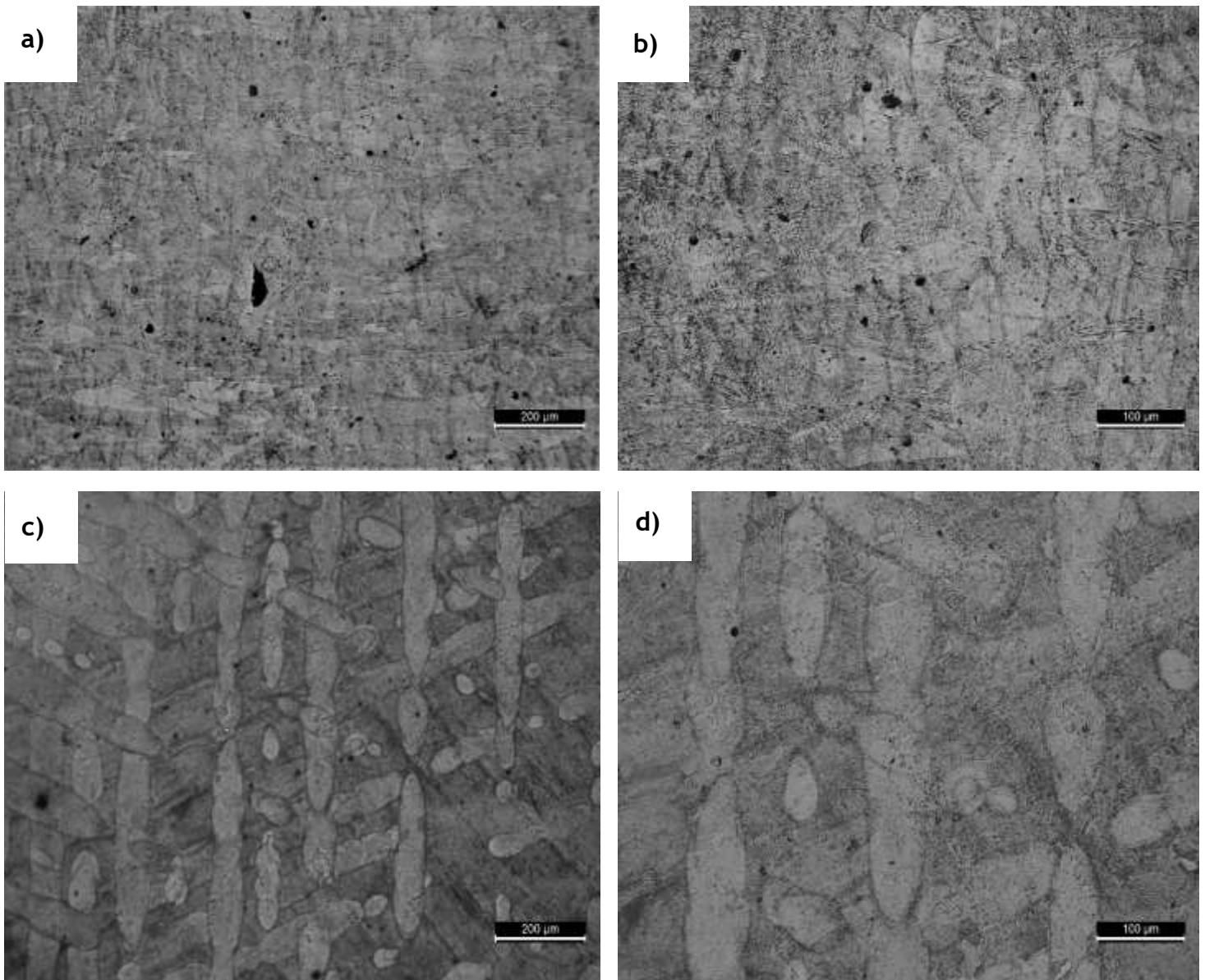
Fig. 39 - OM image of the control batch of VD (a and b) and HoD (c and d).

This images present very little detail when it comes to distinguish its constituents. In this way, SEM/EBSD analysis were made in the same samples and this enabled a more in-depth analysis of the microstructure, being able to identify the differences between the two directions. In figure 42, are presented the microstructures according to the SEM/EBSD analysis and these images show different grain orientation, the vertical sample presents grains with a more elongated shape and the horizontal direction shows a more equiaxial grain. These differences in the grain growth orientation according to the building orientation is also observed in the research developed by D. Deng *et* al. [32] and S. Gorsse *et* al. [54].
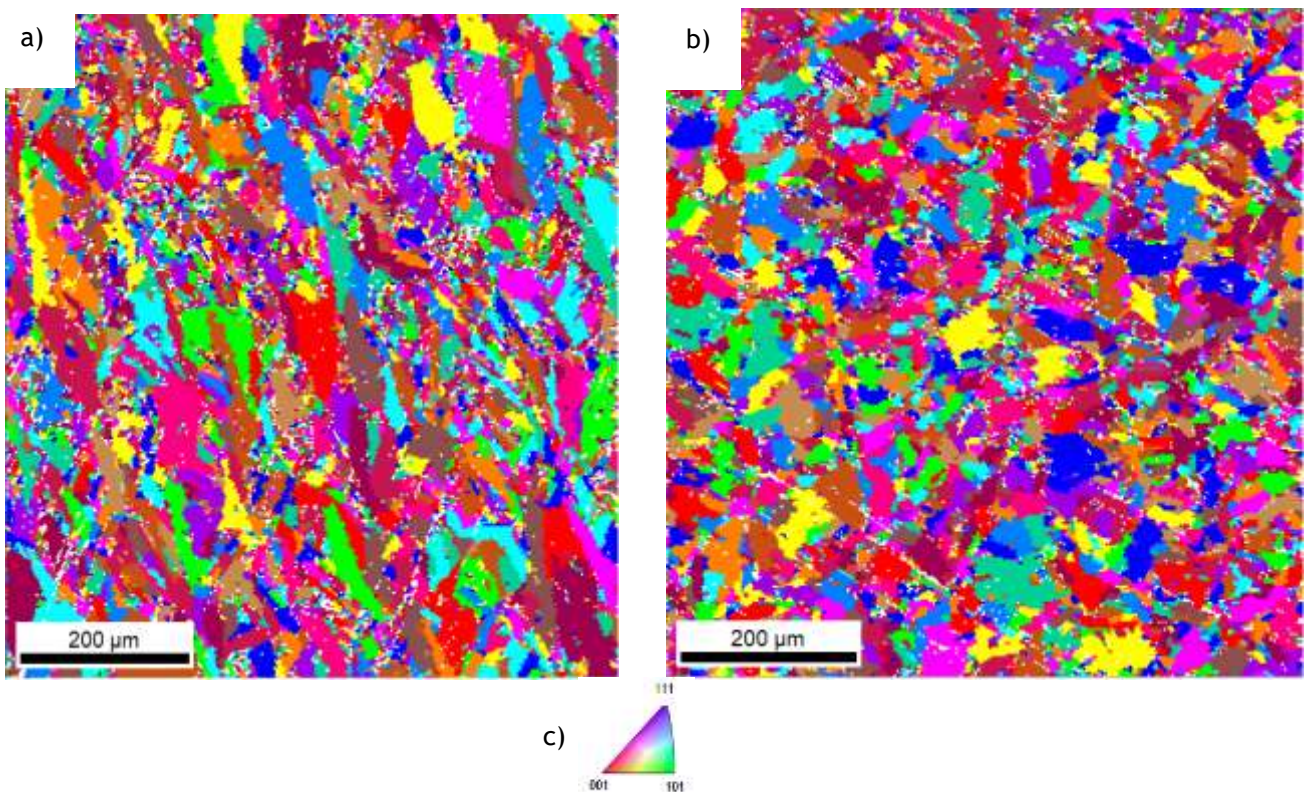
Fig. 40 - SEM/EBSD results concerning the VD (a) and HoD (b) for the control batch c) Inverse polo figure.

These results have answered to one of the most important questions raised in this research, which is why there is a variation in the mechanical properties between the two directions of construction. Making a correlation with the tensile tests, the vertically built samples were tested with the columnar grains parallel to the stress axis, and the horizontally built samples were tested with the stress axis perpendicular to the length of the columnar grains. The higher elongation in VD can

be mainly attributed to the fact that the columnar grains are along the length of the tensile samples [54, 57].

The outcomes concerning the texture detected by the software TSL OIM Analysis 5 are presented in figure 43 This analysis gives as red areas the direction that the grain tends to follow during the crystallization, TD means transversal direction and RD, rolling direction.
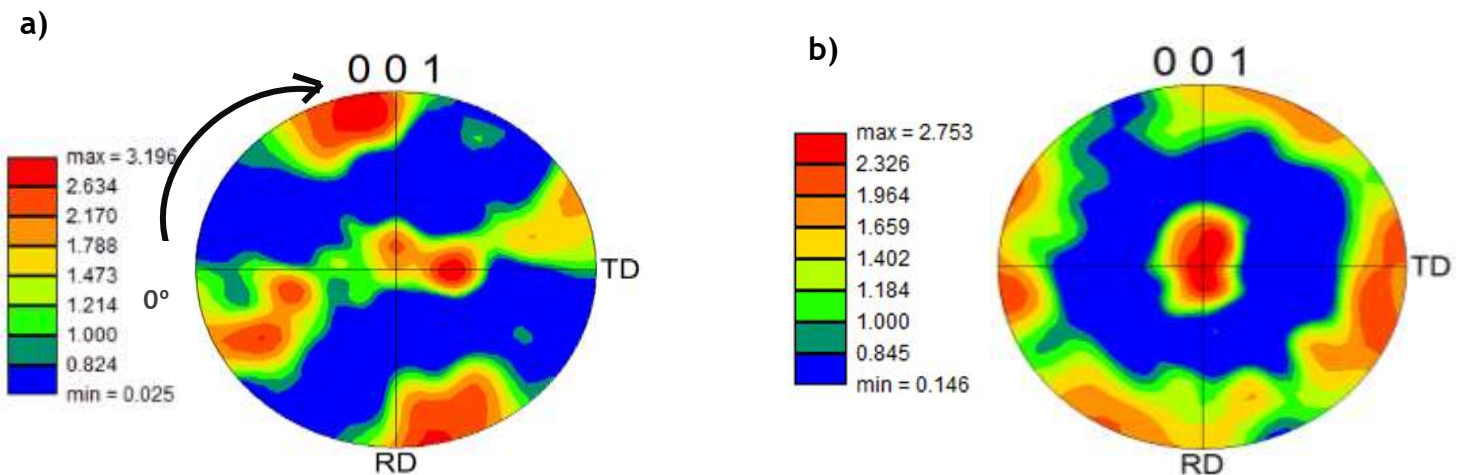
Fig. 41 - Texture analysis given by TSL OIM Analysis 5 software for (a) VD and (b) HoD.

In the first case, there are two main red areas, proving the existence of a preferential growth direction, that so far what it's known is that it's less than 90° from the origin and TD axis. However, using figure 44 a) that represents the grain shape orientation it's possible to affirm that the angle in question is between 70°- 80 °. In this way, the grains grow, approximately, at 70° from TD and at 20 ° from RD. The existence of a preferential direction is in agreement with the appearance of elongated grains in the microstructure. Regarding figure 43-b, there is only one red area in the center, meaning that the grains tend to growth in the 001 direction. Considering, that this sample was built horizontally, the grains crystallization direction follows the build direction. The grain shape orientation of the horizontal specimen (figure 44-b) shows that distribution is well balanced, not displaying a preferential angle. With this, it's natural that the microstructure given by SEM/EBSD presents an equiaxial grain.
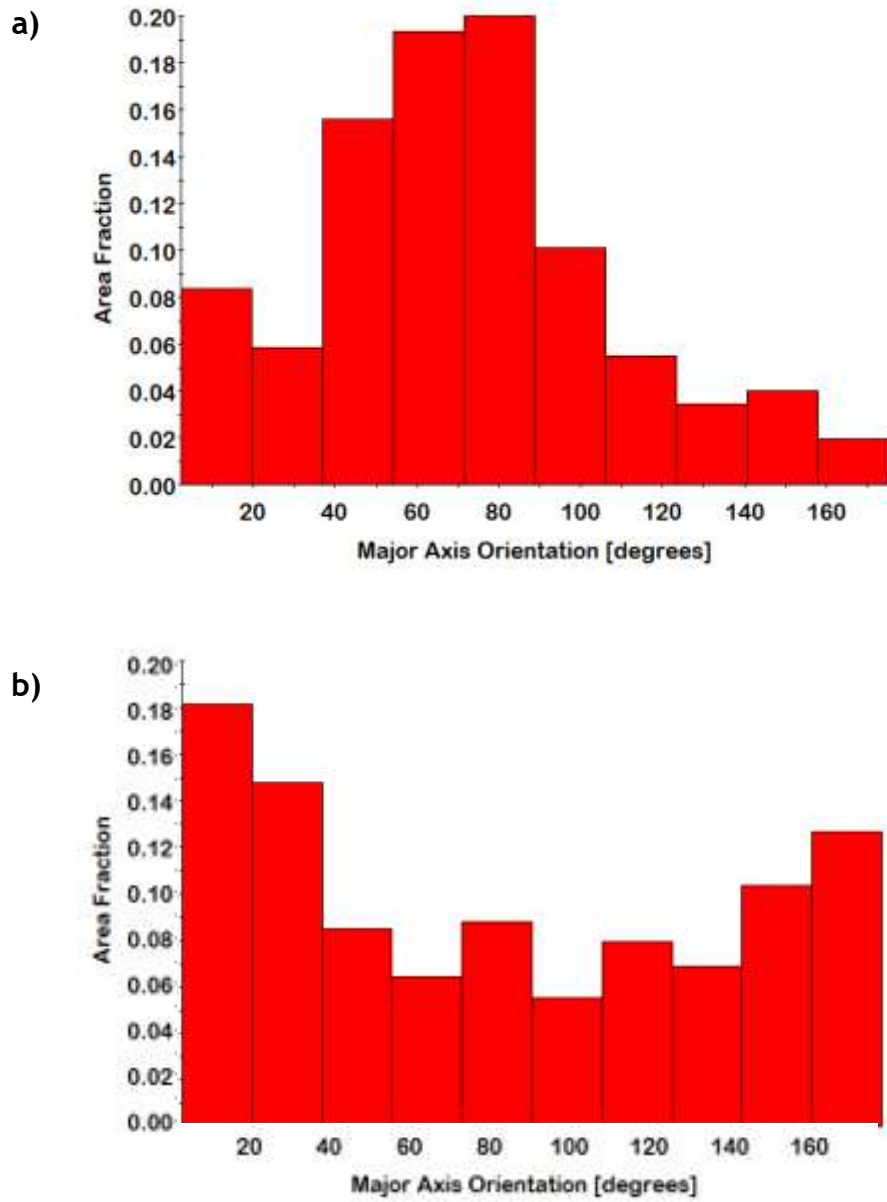
Fig. 42 - Grain shape orientation for (a) VD and (b) HoD.

Conclusions

There has recently been consensus that the unique capabilities offered by AM processes qualify them to be game changing technologies. The design freedom, the ability to produce arbitrarily complex geometries, and reduced material waste, among other benefits, can have transformational roles across many industry sectors such as aerospace, healthcare, and automotive. However, there is also similar consensus among experts and stakeholders that the quality of metallic AM parts is still not sufficient to meet the stringent requirements of these sectors, which hampers the widespread adoption of AM as a viable method of manufacturing. This represents a major barrier toward fully exploiting the unique capabilities that it offers.

One of the main goals of this research was to explore the methods of quality control, focusing on, evaluating CT's accuracy through its comparison with other techniques (OM and Archimedes method). This allows to take one step closer to the qualification of the parts manufactured by AM. Besides, in order to go further in the AM technology, it's crucial to have a fully understanding of the process, its underlying physical mechanism and find out how process parameters affect the microstructure and mechanical properties. In this sense, during this investigation it was also one of the objectives evaluate how the process parameters influenced the microstructures and mechanical properties of the parts.

Firstly, it was shown through the CT results that the porosity values change according to the parameters set in the process, and concerning the cube samples, the sample that stood out for its high porosity value was specimen 23 (4.13% ± 0.37) being a consequence of the low ET applied. Specimen 19 (0.44% ± 0.30) presented an even lower porosity compared to the control samples, due to the lowest DH value applied.

When compared the CT and OM results, concerning the porosity in the same cross section, the results were satisfactory, in the sense, that the porosity observed through pictures was similar as well as porosity percentages. Besides, the type of porosity shown in specimen 23 in the OM pictures was angular, flat defects and voids, proving the lowest sphericity value given by the CT. Additionally, analyzing the relationship between the process parameters and porosity values through the

interaction plots, it's possible to point out that the parameter that provoked the higher deviation from the average values was the ET, particularly, when applying the ET of 40 µs. Still in the interaction plot, it's feasible to affirm that the interaction between all the parameters is strong due to the amount of non-parallel lines, proving that during the process all the parameters act simultaneously.

Regarding the ED studies, it was shown that the porosity decreases with the ED applied until a certain point, namely, 52 J.mm^{-3}, then it presents an approximately constant value of porosity. The inverse happens when it comes to the relative density vs ED, meaning that the relative density increases with the ED until the 83.3 J.mm^{-3} and then it also stabilizes.

Concerning the mechanical properties of the specimens built in two different directions (XY and Z), it's possible to say that, the vertically built ones shows lower strength but higher ductility than the horizontally built sample. The average of UTS value is 925±149 MPa for the VD and 1036±206 MPa for HoD. The strain values are respectively, 28±8 % and 17±6 %. This sample orientation dependence of mechanical properties of the Inconel 718 samples is probably attributed to the different amount of residual stress due to different thermal gradients and dislocations accumulated in the samples. The CT results showed that the presence of porosity affects negatively the strain value, meaning that high porosity results in low strain value. Besides, applying low LP values, such as 100 J.s^{-1} had as a consequence a considerable difference of porosity between the two directions. The HoD showed a high value of porosity probably due to elevated thermal gradients, there may be areas where the powder doesn't re-melt totally due to the lowering of temperature, leading to higher values of porosity.

In the OM analysis, for both directions it's possible to see an overview of the layer structure of horizontal and vertical specimens with the distinct melt pool boundaries. For vertical specimens, the microstructures reflect the laser melt pools that appear predominantly half-cylindrical shape. In the horizontal specimens, the melt pool boundaries have a different shape, showing a cross-hatching scan strategy. Some cellular-dendrites are observed next to melt pool boundaries and its growth is governed by the local thermal condition.

The microstructures according to the EBSD showed that vertical sample presents grains with a more elongated shape and the horizontal direction shows a more equiaxial grain. Moreover, to be certain about the texture of the samples and grain orientation, it's necessary to analyze a significant surface area which did not happen in this case. In other words, the reduced surface area analyzed does not allow clear conclusions to be drawn about the crystallographic texture. What can be mentioned is that, distinct grain orientation will affect the mechanical properties in each direction due to different residual stresses in the microstructure and the fact that the direction of the applied force during the tensile tests according to the grains orientation is different.

Regarding quality control, the CT technique has shown to be a good asset in the AM field because its results were mostly in accordance to the other more common methods. However, it would have been better to analyze a large batch, including for each set of parameters more than one sample. In this case, it would be possible to collect more precise information regarding the uncertainty of the measurements, being easier to identify deviations.

Besides, alongside with other techniques, such us OM and SEM/EBSD, CT proved to be a good complementary technique not only for quality control but also for perceiving the differences in mechanical properties between the two construction directions. In this way, it was possible to establish the relationship that the presence of porosity interferes with the ductility value of the manufactured parts. Besides, to study the effect of process parameters this method is good resource since it can evaluate the porosity distribution and ratio according to a certain set of parameters.

Lastly, it's important to point out that, CT's development has not stagnated, which means that expectations regarding this technique remain high. Improvements are still expected in order to address the drawbacks of this technique, namely measurement time and uncertainty. However, the fact that it is a non-destructive method is an advantage unmatched by other techniques and this makes its adoption ever greater, especially, in the AM field.

Bibliography

1. Blinn, B., et al., *An Investigation of the Microstructure and Fatigue Behavior of Additively Manufactured AISI 316L Stainless Steel with Regard to the Influence of Heat Treatment.* Metals, 2018.

2. Levy, G.N., R. Schindel, and J.P. Kruth, Rapid Manufacturing and rapid tooling with layer manufacturing (LM) tecnhologies, state of art and future perspectives. CIRP Annals, 2003. **52**(2): p. 589-609.

3. Kim, H., et al. (2018). "A review on quality control in additive manufacturing." Rapid Prototyping Journal **24**(3): 645-669.

4. DebRoy, T., et al., *Additive manufacturing of metallic components – Process, structure and properties.* Progress in Materials Science, 2018. **92**: p. 112-224.

5. Edwards, P. and M. Ramulu, *Fatigue performance evaluation of selective laser melted Ti-6Al-4V.* Materials Science and Engineering: A, 2014. **598**: p. 327-337.

6. international, I.A., *ISO_ASTM 52900.* 2015.

7. Mani, M., et al., *Measurement Science Needs for Real-time Control of Additive Manufacturing Powder Bed Fusion Processes.* National Institute of Standards and Technology, 2015.

8. O'Regan, P., et al., *Metal Based Additive Layer Manufacturing: Variations, Correlations and Process Control.* Procedia Computer Science, 2016. **96**: p. 216-224.

9. Mrugalska, B. and E. Tytyk, *Quality Control Methods for Product Reliability and Safety.* Procedia Manufacturing, 2015. **3**: p. 2730-2737.

10. King, W.E., et al., *Laser powder bed fusion additive manufacturing of metals; physics, computational, and materials challenges.* Applied Physics Reviews, 2015. **2**(4): p. 041304.

11. Baturynska, I., O. Semeniuta, and K. Martinsen, *Optimization of Process Parameters for Powder Bed Fusion Additive Manufacturing by Combination of Machine Learning and Finite Element Method: A Conceptual Framework.* Procedia CIRP, 2018. **67**: p. 227-232.

12. ISO/ASTM52900-15, *Standard Terminology for Additive Manufacturing – General Principles – Terminology.* ASTM International, 2015(West Conshohocken, PA).

13. Afonso, J.T.F.G., *Quality control in additive manufacturing - Capacity assessment of non-touching methods*, in *Departamento de engenharia metalúrgica e de materiais*. 2017, Universidade do Porto.

14. Pupo, Y., et al., *Scanning Space Analysis in Selective Laser Melting for CoCrMo Powder.* Procedia Engineering, 2013. **63**: p. 370-378.

15. Hanzl, P., et al., *The Influence of Processing Parameters on the Mechanical Properties of SLM Parts.* Procedia Engineering, 2015. **100**: p. 1405-1413.

16. Yap, C.Y., et al., *Review of selective laser melting: Materials and applications.* Applied Physics Reviews, 2015. **2**(4): p. 041101.

17. Kamath, C., et al., *Density of additively-manufactured, 316L SS parts using laser powder-bed fusion at powers up to 400 W.* The International Journal of Advanced Manufacturing Technology, 2014. **74**(1-4): p. 65-78.

18.   Maarten, v.E., A.B. Farid, and K. Jean-Pierre, *Application of dimensional analysis to selective laser melting.* Rapid Prototyping Journal, 2008. **14**(1): p. 15-22.

19.   Ahmadi, A., et al., *Effect of manufacturing parameters on mechanical properties of 316L stainless steel parts fabricated by selective laser melting: A computational framework.* Materials & Design, 2016. **112**: p. 328-338.

20.   Bikas, H., P. Stavropoulos, and G. Chryssolouris, *Additive manufacturing methods and modelling approaches: a critical review.* The International Journal of Advanced Manufacturing Technology, 2015. **83**(1-4): p. 389-405.

21.   Sculpteo. *Layer thickness in 3D printing: An additive manufacturing basic.* [cited 2018 11th April]; Available from: https://www.sculpteo.com/en/glossary/layer-thickness-definition/.

22.   Gong, H., *Generation and detection of defects in metallic parts fabricated by selective laser melting and electron beam melting and their effects on mechanical properties.* University of Louisville, 2013.

23.   Zhang, B., Y. Li, and Q. Bai, *Defect Formation Mechanisms in Selective Laser Melting: A Review.* Chinese Journal of Mechanical Engineering, 2017. **30**(3): p. 515-527.

24.   Grasso, M. and B.M. Colosimo, *Process defects and in situ monitoring methods in metal powder bed fusion: a review.* Measurement Science and Technology, 2017. **28**(4): p. 044005.

25.   Dr. Bree, M.S., *Non-Destructive Techniques and Technologies for Qualification of Additive Manufactured Parts and Processes: A Literature Review.* Atlantic Research Centre 2015.

26.   Smith, R.J., et al., *Spatially resolved acoustic spectroscopy for selective laser melting.* Journal of Materials Processing Technology, 2016. **236**: p. 93-102.

27.   Mercelis, P. and J.P. Kruth, *Residual stresses in selective laser sintering and selective laser melting.* Rapid Prototyping Journal, 2006. **12**(5): p. 254-265.

28.   Yadroitsev, I. and I. Smurov, *Selective laser melting technology: From the single laser melted track stability to 3D parts of complex shape.* Physics Procedia, 2010. **5**: p. 551-560.

29.   AM, M. *Metal powders – the raw materials.* [cited 2018 11th April]; Available from: http://www.metal-am.com/introduction-to-metal-additive-manufacturing-and-3d-printing/metal-powders-the-raw-materials/.

30.   Lu, Z.L., et al., *Review of main manufacturing processes of complex hollow turbine blades.* Virtual and Physical Prototyping, 2013. **8**(2): p. 87-95.

31.   Wang, X., T. Keya, and K. Chou, *Build Height Effect on the Inconel 718 Parts Fabricated by Selective Laser Melting.* Procedia Manufacturing, 2016. **5**: p. 1006-1017.

32.   Deng, D., et al., *Microstructure and mechanical properties of Inconel 718 produced by selective laser melting: Sample orientation dependence and effects of post heat treatments.* Materials Science and Engineering: A, 2018. **713**: p. 294-306.

33.   Trosch, T., et al., *Microstructure and mechanical properties of selective laser melted Inconel 718 compared to forging and casting.* Materials Letters, 2016. **164**: p. 428-431.

34.   Insights, D. *3D opportunity for quality assurance and parts qualification.* [cited 2018 18th April]; Available from: https://www2.deloitte.com/insights/us/en/focus/3d-opportunity/3d-printing-quality-assurance-in-manufacturing.html.

35.   GAO, *3D printing: opportunities, Challenges, and Policy Implications of Additive Manufacturing*, U.S.G.A. Office, Editor. 2015.

36. international, A. *New Guide for Nondestructive Testing of Additive Manufactured Metal Parts Used in Aerospace Applications.* [cited 2018 18th April]; Available from: https://www.astm.org/WorkItems/WK47031.htm.

37. Spierings, A., M. Schneider, and R. Eggenberger, *Comparison of Density Measurement Techniques for Additive Manufactured Metallic Parts.* Vol. 17. 2011. 380-386.

38. Slotwinski, J.A., E.J. Garboczi, and K.M. Hebenstreit, *Porosity Measurements and Analysis for Metal Additive Manufacturing Process Control.* Journal of Research of the National Institute of Standards and Technology, 2014. **119**: p. 494-528.

39. Thompson, A., I. Maskery, R.K. Leach,, *X-ray computed tomography for additive manufacture a review.* Measurement Science and Technology, 2016.

40. Gapinski, B., et al., *Application of the Computed Tomography to Control Parts Made on Additive Manufacturing Process.* Procedia Engineering, 2016. **149**: p. 105-121.

41. Ziółkowski, G., et al., *Porosity Detection by Computed Tomography.* Pomiary Automatyka Robotyka, 2017. **21**(3): p. 27-34.

42. Probst, G., et al. *Computed tomography: a powerful imaging technique in the fields of dimensional metrology and quality control.* in *SPIE Commercial + Scientific Sensing and Imaging.* 2016. SPIE.

43. *Industrial applications of computed tomography.* CIRP Annals, 2014. **63**(2): p. 655 - 677.

44. Brierley, N., *XCT solution for AM inspection - EPMA release Nick Brierley.* 2017, MTC - Manufacturing technology center.

45. Kruth, J.P., et al., *Computed tomography for dimensional metrology.* CIRP Annals, 2011. **60**(2): p. 821-842.

46. Villarraga-Gómez, H., *X-ray Computed Tomography for Dimensional Measurements.* 2016.

47. Welkenhuyzen, F., et al. (2009). Industrial computer tomography for dimensional metrology: Overview of influence factors and improvement strategies.

48. Wilsnack-Christoph, *Prozessuntersuchungen-zum-selektiven-Laserschmelzen-Diplomarbeit.*, in *Institute of Materials Science.* 2017, Technische Universität Dresden

49. DIN, *DIN 50125: Testing of metallic materials - tensile test pieces.* 2009.

50. Zhou, X., et al., *Balling phenomena in selective laser melted tungsten.* Journal of Materials Processing Technology, 2015. **222**: p. 33-42.

51. Zhou, X., et al., *3D-imaging of selective laser melting defects in a Co-Cr-Mo alloy by synchrotron radiation micro-CT.* Acta Materialia, 2015. **98**: p. 1-16.

52. Mumtaz, K.A. and N. Hopkinson, *Selective Laser Melting of thin wall parts using pulse shaping.* Journal of Materials Processing Technology, 2010. **210**(2): p. 279-287.

53. Rausch, A.M., et al., *Predictive Simulation of Process Windows for Powder Bed Fusion Additive Manufacturing: Influence of the Powder Bulk Density.* Materials, 2017.

54. Gorsse, S., et al., *Additive manufacturing of metals: a brief review of the characteristic microstructures and properties of steels, Ti-6Al-4V and high-entropy alloys.* Science and Technology of Advanced Materials, 2017. **18**(1): p. 584-610.

55. Qiu, C., N.J.E. Adkins, and M.M. Attallah, *Microstructure and tensile properties of selectively laser-melted and of HIPed laser-melted Ti-6Al-4V.* Materials Science and Engineering: A, 2013. **578**: p. 230-239.

56. Zhao, J., et al., *Effect of building direction on porosity and fatigue life of selective laser melted AlSi12Mg alloy.* Materials Science and Engineering: A, 2018. **729**: p. 76-85.

57. Vilaro, T., C. Colin, and J. D. Bartout, *As-Fabricated and Heat-Treated Microstructures of the Ti-6Al-4V Alloy Processed by Selective Laser Melting.* Vol. 42. 2011. 3190-3199.

58. weibull. *Introduction to Design of Experiments (DOE).* 2008 [cited 2018 24th may]; Available from: http://www.weibull.com/hotwire/issue84/hottopics84.htm.

59. Steam, M. *Design of Experiments (DOE).* [cited 2018 25th may]; Available from: https://www.moresteam.com/toolbox/design-of-experiments.cfm.

60. Handbook, E.S. *Central Composite Designs (CCD).* [cited 2018 25th may]; Available from: https://www.itl.nist.gov/div898/handbook/pri/section3/pri3361.htm

Annexes

Annex A – Design of experiences chapter.

Figures index

Table index

Design of Experiences (DoE)

Much of our knowledge about products and processes in engineering and scientific disciplines is derived from experimentation, being, an experiment a series of tests in which the input variables are changed according to a given rule in order to identify the reasons for the changes in the output response [48, 58] (1,2).

The objectives of the experiment include:

- Identifying relationships between cause and effect.
- Providing an understanding of interactions among causative factors.
- Determining the levels at which to set the controllable factors (product dimension, alternative material, alternative designs, etc.) in order to optimize reliability.
- Minimizing experimental error (noise).
- Improving the robustness of the design or process to variation [58] (2).

Experimental design, is the name given to the techniques used for guiding the choice of the experiments to be performed in an efficient way. Designed experiments are much more efficient than one-factor-at-a-time experiments, which involve changing a single factor at a time to study the effect of the factor on the product or process. While the one-factor-at-a-time experiments are easy to understand, they do not allow the investigation of how a factor affects a product or process in the presence

of other factors. Many times the interaction effects, this means, the relationship between several factors, are more important than the effects of individual factors. This is because the application environment of the product or process includes the presence of many of the factors together instead of isolated occurrences of single factors at different times [58, 59] (2,3).

There are three concepts to consider in experimental design, namely, factor (inputs to the process), levels (settings of each factor in the study) and response (output of the experiment). Besides, to successfully, apply experimental design, several steps need to be taken (fig. annex 1). In this research the main problem is the part's porosity, the goal is to correlate process parameters with the porosity percentage and for that it's necessary to define a strategy. With this, the DoE method adopted is called, *Central Composite* Designs (CCD) [59] (3).
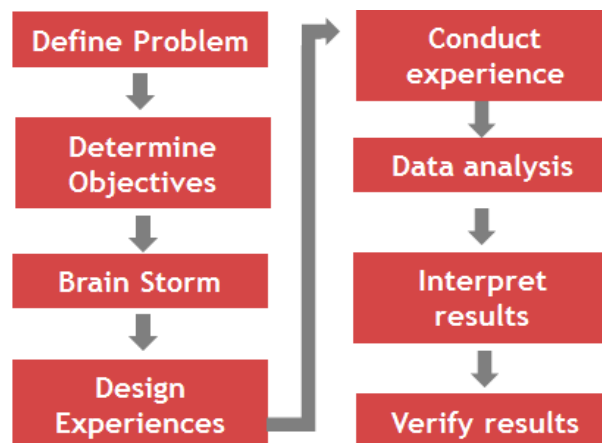
Fig. Annex 1 - Design of Experience process [59] (3).

Central Composite Designs

A Box-Wilson Central Composite Design, commonly called 'a central composite design,' consists in a full factorial and partial factorial designs to which the central point and the star points are added (Fig. Annex 2). A CCD always contains twice as many star points as there are factors in the design. The star points represent new extreme values (low and high) for each factor in the design. Put this, the star points are the sample points in which all the parameters but one are set at the mean level "m". The value of the remaining parameter is given in terms of distance from the central point. If the distance from the center to a factorial point is ±1 unit for each

factor, the distance from the center to a star point is $|\alpha| > 1$. The precise value of α depends on certain properties desired for the design and on the number of factors involved [48, 60] (1,4).
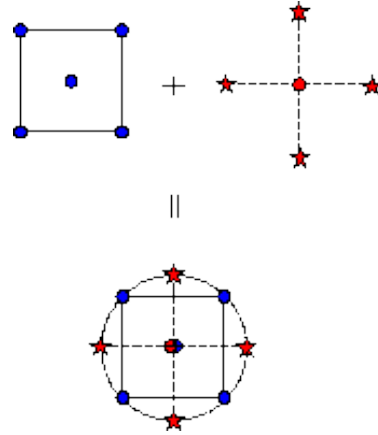
Fig. Annex 2 - Generation of a Central Composite Design for Two Factors [60] (4).

CCD design plans can be divided into three types: Central Composite Circumcribed Design (CCC), when the star points are located outside, Central Composite Inscribed (CCI), the stars are within and Central Composite Face Centered (CCF), the stars are on the surface. The different types and some characteristics are shown in table annex 1 [48, 60] (1, 4).

Table Annex 1 - Comparison of the Three Types of Central Composite Designs [48] (1).
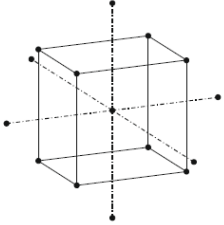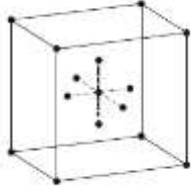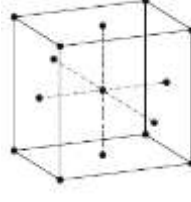
	CCC	CCI	CCF
3D model			
Levels for each factor	5	5	3
a value	>1	<1	=1

The designs CCC and CCI are rotatable in contrast to the CCF. The star points lie on a circle or a sphere, which are spanned by the corner points of the system. To ensure the rotation, there is the magnification factor α, which depends on the number of experiments and thus on the number of factors k. This is calculated using the following formula [48, 60] (1, 4):

$$\alpha = (number\ of\ factorial\ runs)^{1/4} \tag{1}$$

If the factorial is a full factorial, then:

$$\alpha = (2K)^{1/4} \tag{2}$$

Table annex 2 illustrates some typical values of α as a function of the number of factors [60] (4).

Table Annex 2 - Typical values of 'a' as a function of the number of factors [60] (4).

Number of Factors	Factorial Portion	Scaled Value for α Relative to ±1
2	2^2	$2^{2/4} = 1.414$
3	2^3	$2^{3/4} = 1.682$
4	2^4	$2^{4/4} = 2.000$
5	2^{5-1}	$2^{4/4} = 2.000$
5	2^5	$2^{5/4} = 2.378$
6	2^{6-1}	$2^{5/4} = 2.378$
6	2^6	$2^{6/4} = 2.828$

Bibliopgraphy

(1) Wilsnack-Christoph, *Prozessuntersuchungen-zum-selektiven-Laserschmelzen-Diplomarbeit.*, in *Institute of Materials Science*. 2017, Technische Universität Dresden

(2) weibull. *Introduction to Design of Experiments (DOE)*. 2008 [cited 2018 24th may]; Available from: http://www.weibull.com/hotwire/issue84/hottopics84.htm.

(3) Steam, M. *Design of Experiments (DOE)*. [cited 2018 25th may]; Available from: https://www.moresteam.com/toolbox/design-of-experiments.cfm.

(4) Handbook, E.S. *Central Composite Designs (CCD)*. [cited 2018 25th may]; Available from: https://www.itl.nist.gov/div898/handbook/pri/section3/pri3361.htm

Annex B - YXLON reconspooler Parameters.

Parameter	Description
Iso Voxel	The "reconstruction volume size" parameter is automatically set to the horizontal pixel count according to the current detector settings.
Reconstruction Volume Size	Size of the reconstruction volume. Depending on the set size, there is a shorter runtime for a lower level of detail or a longer runtime for a higher level of detail. The resulting voxel size is displayed under the slide control. It results from the geometric enlargement, the detector size and the set volume size.
Beam Hardening Correction	Reducing beam hardening artefacts. After this function has been activated, a filter - as well as an object material - can be selected. In addition, the thickness of the filter material can be set.
32 Bit float Volume	The reconstructed volume is represented by 32-bit floating-point values. When the option is active, the reconstructed volume requires twice as much memory. The option should be used when there are bright objects in the reconstructed volume.
Truncation Correction	With the option enabled, an attempt is made to reduce barreling effects by extrapolation. The option should be enabled when the inspection object partially moves out of the image during rotation or, due to sub-optimum illumination, barreling effects can be seen in the reconstructed volume.
Noise Reduction (Projection Space)	Enable noise reduction on the projections. Noise reduction can be adjusted with the following two parameters, Range Sigma and Spatial Sigma.
Range Sigma	Strength of the edges that should be retained despite smoothing. Higher values produce a stronger smoothing effect.
Spatial Sigma	Strength of the edge retaining smoothing effect.
Noise Reduction (Volume Space)	Enable noise reduction on the reconstructed volume. Noise reduction can be adjusted with the following three parameters, Iteration, P1 and P2.
Iterations	Number of filtering iterations. Higher values produce a stronger smoothing effect.
P1	Width at half the maximum of the influence curve used for edge retaining. Higher values produce a stronger smoothing effect.
P2	Offset of the influence curve used for edge retaining. Higher values produce a stronger smoothing effect.
Ring Artifact Reduction	Enable "retrospective" ring object correction. In contrast to the option in the scans, this correction does not change the projections permanently. As a result, an initial "strong" correction can be reversed even with repeated reconstruction. The stronger the objects expected, the higher the parameter must be set. A higher value, however, is at the cost of resolution in the reconstructed volume. For the ring object correction values between 0 and 3 can be set: – 0: Correction switched off. – 1: Rings with a width up to 2 pixels can be reduced.

	– 2: Rings with a width up to 4 pixels can be reduced.
	– 3: Rings with a width up to 8 pixels can be reduced.
	Large values can cause even non-annular structures to be smeared.
Bad Pixel Reduction	Enable correction of individual defective pixels in the projections. The correction can be adjusted with the following four parameters, Filter size, Global Threshold, Low Domain Deviation and High Domain Deviation.
Filter Size	Edge length in pixels of the region used for bad pixel reduction.
Global Threshold	Grey value for the division in the "lower domain" (dark areas) and the "upper domain" (bright areas).
Low Domain Deviation	If a pixel of the lower domain deviates by this percentage from the mean value of the region defined in the "Filter size" parameter, its value is replaced by the median of the neighboring pixels.
High Domain Deviation	If a pixel of the upper domain deviates by the set percentage from the mean value of the region defined in the "Filter size" parameter, its value is replaced by the median of the neighboring pixels.
Median Filter	Size of the median filter mask in pixels. Larger values provide a stronger filter effect.

Annex C - Porosity/Inclusion analysis window.
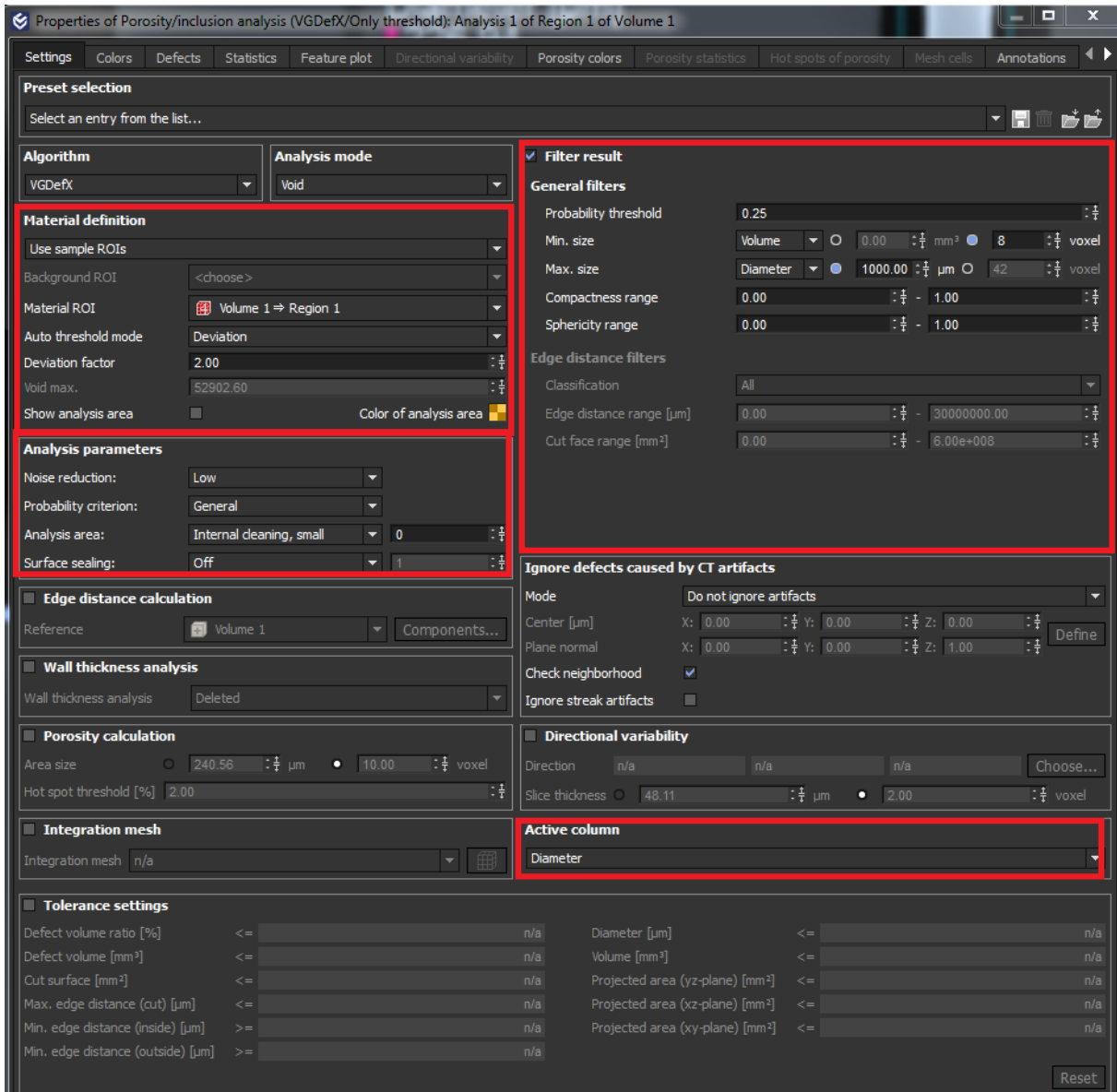
Annex D - Porosity analysis parameters of the density cubes and tensile strength samples.

Samples	Algorithm	Analysis mode	Material definition			Analyis Parameters			Filter Result		
			Use Determined Surface / Auto Threshold mode	Desviation Factor		Noise Reduction	Probability Criterion	Analysis Area	Probability Threshold	Min. Size Diameter (voxel)	Max. Size Diameter (voxel)
Density Cubes	VGDefX	Voide	Desviation	2		low	General	From surface (as seen)	0,25	1	44
Tensile Strength Samples	VGDefX	Voide	Desviation	2		low	General	ROI from Volume	0,25	1	42

Annex E - Individual parameters main efects on porosity.

Main Effects Plot of Porosity by P_Laser
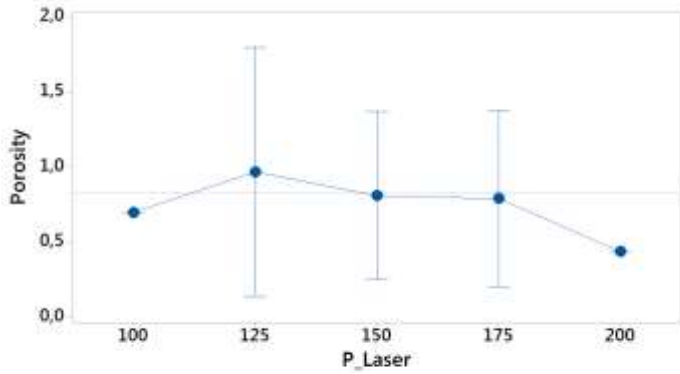
Statistics	100	125	150	175	200
N	1	8	14	8	1
Mean	0,7	0,97	0,81143	0,7925	0,44
95% CI	(*; *)	(0,143; 1,	(0,252; 1,	(0,206; 1,	(*; *)
StDev	*	0.98952	0.96853	0.70213	*

Main Effects Plot of Porosity by d_Point
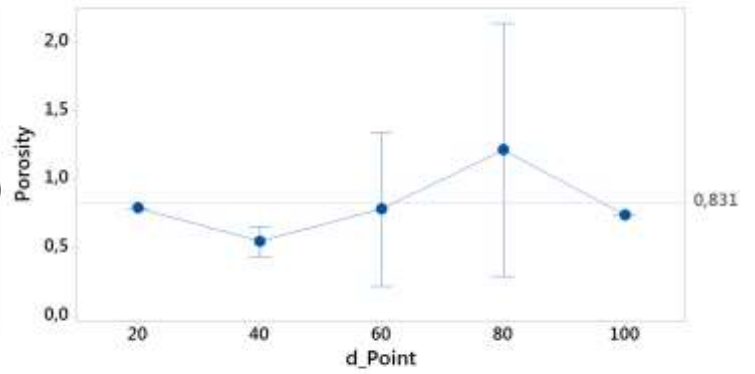
Statistics	20	40	60	80	100
N	1	8	14	8	1
Mean	0,79	0,5475	0,78357	1,215	0,74
95% CI	(*; *)	(0,437; 0,	(0,221; 1,	(0,292; 2,	(*; *)
StDev	*	0.13264	0.97383	1.1036	*

Main Effects Plot of Porosity by t_exp
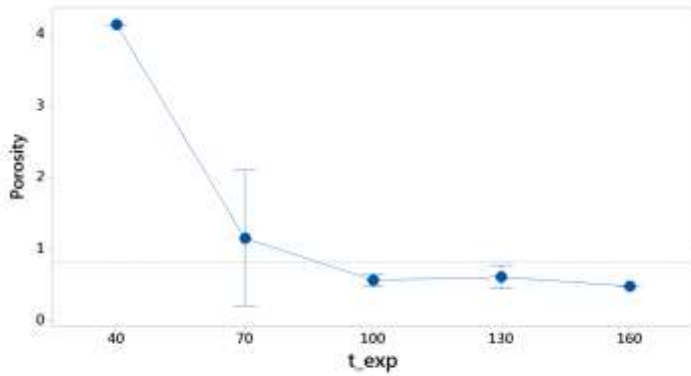
Statistics	40	70	100	130	160
N	1	8	14	8	1
Mean	4,14	1,1513	0,56286	0,61125	0,48
95% CI	(*; *)	(0,204; 2,	(0,477; 0,	(0,446; 0,	(*; *)
StDev	*	1.1334	0.14953	0.19723	*

Main Effects Plot of Porosity by d_hatch
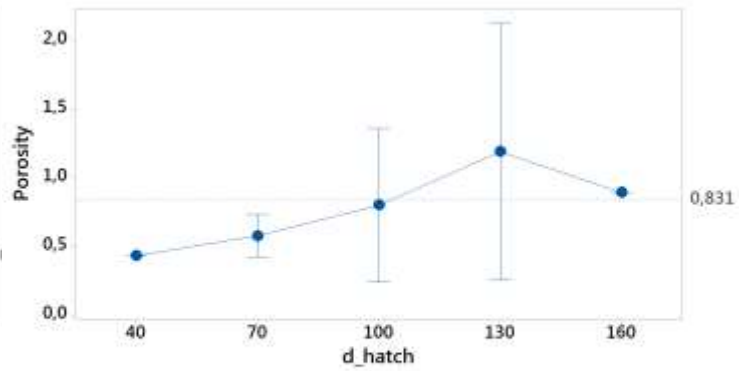
Statistics	40	70	100	130	160
N	1	8	14	8	1
Mean	0,43	0,575	0,79857	1,1875	0,89
95% CI	(*; *)	(0,421; 0,	(0,239; 1,	(0,256; 2,	(*; *)
StDev	*	0.18393	0.96838	1.1144	*